© 2021. Published by The Company of Biologists Ltd | Journal of Cell Science (2021) 134, jcs256537. doi:10.1242/jcs.256537

RESEARCH ARTICLE

The role of *Aspergillus nidulans* polo-like kinase PlkA in microtubule-organizing center control

Xiaolei Gao[1], Saturnino Herrero[1], Valentin Wernet[1], Sylvia Erhardt[2], Oliver Valerius[3], Gerhard H. Braus[3] and Reinhard Fischer[1,*]

ABSTRACT

Centrosomes are important microtubule-organizing centers (MTOC) in animal cells. In addition, non-centrosomal MTOCs (ncMTOCs) have been described in many cell types. The functional analogs of centrosomes in fungi are the spindle pole bodies (SPBs). In *Aspergillus nidulans*, additional MTOCs have been discovered at septa (sMTOC). Although the core components are conserved in both MTOCs, their composition and organization are different and dynamic. Here, we show that the polo-like kinase PlkA binds the γ-tubulin ring complex (γ-TuRC) receptor protein ApsB and contributes to targeting ApsB to both MTOCs. PlkA coordinates the activities of the SPB outer plaque and the sMTOC. PlkA kinase activity was required for astral MT formation involving ApsB recruitment. PlkA also interacted with the γ-TuRC inner plaque receptor protein PcpA. Mitosis was delayed without PlkA, and the PlkA protein was required for proper mitotic spindle morphology, although this function was independent of its catalytic activity. Our results suggest that the polo-like kinase is a regulator of MTOC activities and acts as a scaffolding unit through interaction with γ-TuRC receptors.

KEY WORDS: *Aspergillus*, Polo like kinase, Microtubules, ApsB, SPB, sMTOC, PcpA, γ-TuRC, γ-TuCRs, Mto1, Mto2

INTRODUCTION

Microtubules (MTs), along with actin and septins comprise the cell cytoskeleton in most eukaryotic cells. The cytoskeleton is essential in many cellular processes such as cell division, intracellular transport or polar growth. MTs are nucleated from specialized structures, called 'microtubule-organizing centers' (MTOCs). One century ago, the centrosome was identified as the primary MTOC in animals. It is composed of two centrioles and is surrounded by pericentriolar material (PCM) (Bornens, 2012; Wilson, 1925). Its functional analog in fungi, the spindle pole body (SPB), is a multilayered structure embedded in the nuclear envelope that nucleates MTs on both the cytoplasmic and the nuclear face (Jaspersen and Winey, 2004).

Despite fundamental structural differences between centrosomes and SPBs, they share many common molecular components and regulators. The key nucleator γ-tubulin was discovered in the filamentous fungus *Aspergillus nidulans* and is conserved in all eukaryotes (Martin et al., 1997; Oakley et al., 1990; Oakley and Oakley, 1989; Prigozhina et al., 2004). γ-tubulin together with several γ-tubulin complex proteins (GCPs) assemble into a ring structure and initiate MT polymerization (Liu et al., 2020; Teixidó-Travesa et al., 2012; Zheng et al., 1995). Three components, γ-tubulin, GCP2 and GCP3 comprise a core structure, named the γ-tubulin small complex (γ-TuSC) (Kollman et al., 2010). This complex is found in SPBs of *Saccharomyces cerevisiae* (Knop and Schiebel, 1997). In the fission yeast *Schizosaccharomyces pombe* and higher eukaryotes, the complex is larger, includes additionally GCP4, GCP5, GCP6 and a recently discovered new component, MOZART, and is termed the γ-tubulin ring complex (γ-TuRC) (Cota et al., 2017; Masuda and Toda, 2016). A recent study of a MOZART1 ortholog in *A. nidulans* revealed an asymmetric composition of SPBs with γ-TuRCs at the inner and γ-TuSCs at the outer plaque (Gao et al., 2019).

γ-tubulin complexes are regulated by various factors that recruit γ-tubulin complexes to different cellular sites and control MT nucleation activity. The recruiting proteins are often named γ-tubulin complex receptors (γ-TuCRs). The number of receptor proteins increases from yeast to human. Although lacking centrioles, yeasts share the PCM modules with animals, such as pericentrin and CDK5RAP2, which anchor γ-TuSC/γ-TuRC to the SPB/centrosome (Ito and Bettencourt-Dias, 2018). The *S. cerevisiae* SPB has two receptors, $Spc110^{pericentrin}$ and $Spc72^{CDK5RAP2}$ (mammalian homolog names indicated in superscript), targeting γ-TuSCs to the inner (nuclear) and outer (cytoplasmic) plaques of SPBs, respectively (Knop and Schiebel, 1998; Nguyen et al., 1998; Souès and Adams, 1998). Spc72 and its orthologs Mto1 in *S. pombe* and ApsB in *A. nidulans* belong to the CM1-MASC family proteins. They contain an N-terminal centrosomin motif 1 (CM1) that is essential for interacting with γ-TuSC, and a C-terminal MASC domain responsible for anchorage to MTOC sites (Lin et al., 2015; Samejima et al., 2010; Sawin et al., 2004). Spc110 (Pcp1 in *S. pombe* and PcpA in *A. nidulans*) belongs to the SPM-CM1-PACT family and contains two conserved motifs important for MT nucleation activation (SPM and CM1 domains are also present in human pericentrin) as well as a C-terminal MTOC-targeting PACT domain (Flory et al., 2002; Kollman et al., 2010; Lin et al., 2014). Interestingly, *S. pombe* and *A. nidulans* have two outer plaque receptors, $ApsB^{Mto1}$ and $Spa18^{Mto2}$, and one inner plaque receptor, $PcpA^{Pcp1}$ (Suelmann et al., 1998; Zekert et al., 2010; Zhang et al., 2017).

The centrosome/SPB duplicates once per cell cycle to form two competent MTOCs for assembly of mitotic spindles to ensure proper nuclear division. It is known that increased numbers of centrosomes or mutations in centrosomal proteins can lead to cancer and microcephaly (Gönczy, 2015; Nigg and Raff, 2009). The timing

[1]Karlsruhe Institute of Technology (KIT) - South Campus, Institute for Applied Biosciences, Dept. of Microbiology, Fritz-Haber-Weg 4, D-76131 Karlsruhe, Germany. [2]Karlsruhe Institute of Technology (KIT) - South Campus, Zoological Institute, Fritz-Haber-Weg 4, D-76131 Karlsruhe, Germany. [3]University of Göttingen, Dept. of Microbiology, Justus-von-Liebig-Weg 11 37077 Göttingen, Germany.

*Author for correspondence (reinhard.fischer@KIT.edu)

G.H.B., 0000-0002-3117-5626; R.F., 0000-0002-6704-2569

Handling Editor: David Glover
Received 29 October 2020; Accepted 19 July 2021

Journal of Cell Science (2021) 134, jcs256537. doi:10.1242/jcs.256537

of centriole/SPB duplication is tightly regulated by the cell cycle kinase cyclin-dependent kinase 1 (Cdk1) and polo-like kinases (Plks) both in animals and yeasts (Elserafy et al., 2014; Habedanck et al., 2005; Zitouni et al., 2016). Plks are known to play multiple roles in mitotic entry, progression and mitotic exit, DNA-damage checkpoint control and cytokinesis (Archambault and Glover, 2009; Glover, 2005; Liu and Maller, 2005; Smits et al., 2000; Takaki et al., 2008). The human genome encodes five Plks (Plk1–Plk5) that are classified into three subfamilies. Plk1, the most ancient member, is conserved in most eukaryotes except higher plants (Zitouni et al., 2014). Human Plk1 is involved in mitotic entry control, is required for cytokinesis and is essential for centrosome maturation through phosphorylating pericentrin (Lee and Rhee, 2011; Petronczki et al., 2008). *Drosophila* Polo (the Plk1 homolog) enables PCM recruitment to centrosomes via phosphorylation of the CDK5RAP2 homolog Cnn (Conduit et al., 2014) and Sas-4 (Ramani et al., 2018). Plk4 only exists in species with centrioles, where it is involved in centriole biogenesis via phosphorylating its binding partner STIL (Arquint et al., 2015; Moyer et al., 2015). Plk2, Plk3 and Plk5 belong to another subfamily that is less characterized and carries out fewer functions, mostly related to cell differentiation (Zitouni et al., 2014).

Budding and fission yeast have a single Plk1 ortholog, Cdc5 in budding yeast and Plo1 in fission yeast, that play similar roles at mitotic SPBs and cytokinesis sites. *S. cerevisiae* Cdc5 is essential and promotes mitotic exit and cytokinesis through MEN and FEAR networks (Hu et al., 2001; Rahal and Amon, 2008; Song and Lee, 2001). In addition, Cdc5 regulates SPB duplication and mitotic progression through G2/M transition (Avena et al., 2014; Elserafy et al., 2014; Sakchaisri et al., 2004). There is less evidence that Cdc5 drives the MT nucleation pathway directly (Lee et al., 2005). Instead, phosphorylation of Spc110 by the cell-cycle-regulating kinases Mps1 and Cdk is important for promoting Spc110 oligomerization (Lin et al., 2014). Spc72 is one of the Cdc5 substrates and can be phosphorylated *in vitro* (Snead et al., 2007). Similar to Cdc5, *S. pombe* Plo1 is essential for septation initiation network (SIN)-mediated cytokinesis (Tanaka et al., 2001). Additionally, Plo1 plays important roles in mitotic entry and SPB insertion into the nuclear envelope during mitosis (Fong et al., 2010; Wälde and King, 2014). *A. nidulans* encodes only one polo-like kinase, PlkA. It is the largest member of the family and is phylogenetically very distant from other Plk1s (Bachewich et al., 2005). By contrast, phylogenetic analysis places PlkA close to Plk4 (Mogilevsky et al., 2012). The PBD domain of PlkA still contains the conserved residues of Plk1 that are important for phospho-substrate recognition. As a big difference to yeasts, PlkA has lost its essential roles (Mogilevsky et al., 2012) in development and cytokinesis. *A. nidulans* PlkA, hence, could be an ancient protein combining more than one Plk functions that were separated during evolution to different proteins.

Although Plk1 plays important roles in cell cycle control and cytokinesis from yeast to human, the exact contribution to MT nucleation and localization of γ-tubulin complexes is not yet fully understood. Here, we studied the role of the sole polo-like kinase PlkA in MTOC regulation in *A. nidulans*. This organism is of particular interest, because at least two different MTOCs have been described, SPBs and MTOCs associated with septa (sMTOCs) (Konzack et al., 2005; Xiong and Oakley, 2009; Zhang et al., 2017). In addition, the SPB is composed of γTuSC at the outer plaque with ApsB and Spa18 as receptors, and of γTuRC at the inner plaque with PcpA as a receptor. Last but not least, the number of γTuSC and γTuRC units is very dynamic and changes throughout the cell cycle (Gao et al., 2019). These features raise the interesting questions how SPB outer and inner plaque complexes are oppositely regulated throughout the cell cycle and if sMTOC γTuRCs are coordinately regulated with the outer or the inner plaque of SPBs or whether they are independent of cell cycle control. In this study, we present evidence that PlkA coordinates SPB and sMTOC activities via phosphorylating and recruiting γTuCRs. Thus, this study adds new knowledge to the functions of polo-like kinases in lower eukaryotes and may provide novel aspects for the discussion of the origin and expansion of Plks in evolution.

RESULTS

sMTOC activity is regulated during the cell cycle and evidence for polo-like kinase as a potential regulator

MT generation in fungi at the outer and the inner plaque of SPBs is strictly coordinated with the cell cycle. At the onset of mitosis, in *A. nidulans* cytoplasmic MTs disassemble, and the mitotic spindles develop. As mitosis progresses to anaphase, cytoplasmic MTs (astral MTs) reassemble, followed by mitotic spindle disassembly in telophase. It has been suggested that MT catastrophe rates determine the number of cytoplasmic MTs (Szewczyk and Oakley, 2011). MT growth from nucleation sites is determined by a balance between assembly and disassembly rates. In addition, changes in MT nucleation abilities may contribute to the formation of the MT cytoskeleton. Indeed, changes of the numbers of cytoplasmic MTs are accompanied by changes of the number of γ-TuRC complexes at SPBs (Gao et al., 2019). However, much less is known about the dynamics of septal MTOCs. In order to analyze whether septal MTOCs are also regulated during the cell cycle and if their MT-polymerizing activtiy is synchronized with the activity of SPBs, we used the MT plus-end tracking kinesin KipA (Konzack et al., 2005). The GFP–kinesin fusion protein was co-expressed with mCherry-labeled α-tubulin. We analyzed a hyphal compartment undergoing mitosis adjacent to a compartment in interphase and observed KipA comets moving only from septa towards the interphase (Fig. 1A) but not towards the mitotic spindle compartment. This indeed suggests co-regulation of sMTOCs and the outer plaque of the SPB. In contrast, the inner plaque of the SPB of the mitotic compartment was active and produced the spindle MTs. To further confirm the phenomenon, a *bimE7* (for 'block in mitosis') mutant was used to block the cell in mitosis (James et al., 1995). At the restrictive temperature most compartments were blocked in mitosis, as indicated by mitotic spindles, but some compartments escaped the block and were in interphase. Whereas MTs clearly emanated from the cytoplasmic side of the septa of the interphase compartment, the sMTOCs in the adjacent mitotic compartments appeared inactive, although some astral MTs were visible (Fig. S1A). The fact that, in the same cytoplasm, astral MTs appear to grow, whereas MTs from sMTOCs are still absent, suggests that sMTOC activity is blocked and responsible for the observed lack of MTs rather than a change of other parameters influencing MT formation and numbers.

If the outer SPB plaque and sMTOCs are co-regulated, the question arises as to which regulators could be involved. In budding yeast, nearly all SPB-associated proteins are modified through phosphorylation during the cell cycle, including the γ-TuSC and its receptors Spc72 and Spc110 (Keck et al., 2011; Lin et al., 2014; Pereira et al., 1998; Vogel et al., 2001). Anticipating that the same regulation takes place in *A. nidulans*, we considered three kinases to be involved in the regulation of the activity of sMTOCs. The kinase NIMA is essential for mitotic entry (Morris, 1975; Osmani et al., 1987; Shen et al., 2014), aurora A is essential for the spindle assembly checkpoint (De Souza et al., 2017) and the polo-like

Journal of Cell Science (2021) 134, jcs256537. doi:10.1242/jcs.256537

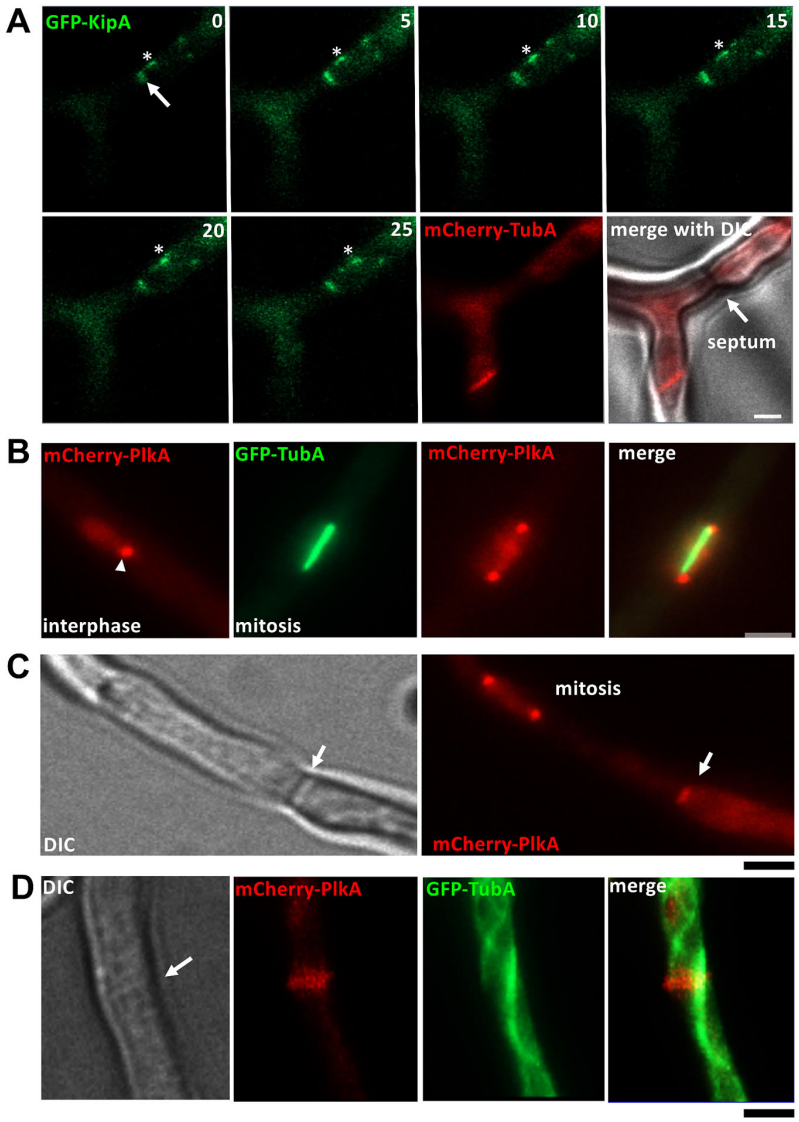

Fig. 1. Observation of sMTOC activities during mitosis and localization patterns of PlkA. (A) The activities of sMTOCs are regulated during the cell cycle in *A. nidulans*. Observation of two hyphal compartments. Whereas the lower one performs mitosis, the upper right one is in interphase. sMTOCs are actively polymerizing MTs from the septum towards the cytoplasm in the interphase compartment. The MT plus-end tracking protein GFP–KipA was followed in a strain where MTs were labeled with mCherry. Strain SXW1 [*alcA(p)::GFP::kipA*; *alcA(p)::mCherry::tuba*] was grown in 8-well u-slides at 28°C overnight for long-term observation. Time-lapse images were taken every 5 s at room temperature. Arrows point to septa. The numbers indicate the time in seconds. The asterisks indicate the MT plus ends. (B,C) Localization of PlkA at SPBs and sMTOCs throughout the cell cycle. (B) Localization of PlkA to nuclei and SPBs at G2 and to mitotic spindles and SPBs at metaphase. The arrowhead indicates SPBs. Strains SXL158 [*alcA(p)::mCherry::plkA*] and SXL176 [*alcA(p)::mCherry::plkA*; *alcA(p)::GFP::tuba*] were incubated in MM (2% glycerol) at 28°C overnight and observed. (C) PlkA remains at septa during mitosis (arrows). Strain SXL158 or SXL176 was used. (D) PlkA localizes to the forming septum. Arrow indicates the position of a forming septum. Strain SXL176 were treated and imaged as above. Images are representative from three independent experiments. Scale bars: 2 µm.

kinase PlkA is important, but not essential, for hyphal development (Mogilevsky et al., 2012). NIMA and Aurora A transiently localize at mitotic spindle zones and relocate to septa during specific phases, while PlkA is associated with SPBs throughout the whole cell cycle, with septal localization unknown (Bachewich et al., 2005; De Souza et al., 2017; Shen et al., 2014). In order to test which kinase could be involved in MTOC activity control, we performed preliminary interaction studies of the kinases with ApsB using the bimolecular fluorescence complementation (BiFC) system (data not shown and see below). Because this assay was positive for the combination of PlkA and ApsB, we focused on PlkA for further investigations.

PlkA localizes at SPBs and sMTOCs throughout the cell cycle and is recruited to forming septa prior to ApsB

To get first insights of PlkA functioning in MTOCs, we asked whether PlkA localizes at SPBs and septal MTOCs *in vivo*. PlkA was tagged with mCherry at the N-terminus, placed under the control of the *alcA*-promoter and introduced into a strain expressing GFP-labeled TubA. mCherry–PlkA was always observed as dot-like structure at nuclei suggesting SPB association. During mitosis, both SPBs were labeled and, in addition, mitotic spindles were decorated, which is consistent with previous results (Fig. 1B) (Bachewich et al., 2005). As a new finding, PlkA was observed permanently at septa, even in mitotic cells (Fig. 1C). Thus, PlkA localizes at SPBs and sMTOCs throughout the whole cell cycle. We also generated a strain with GFP fused at the 3′ end of PlkA under *alcA* promoter control and found that septal localization was lost (Fig. S1B). The C-terminus appears to be important for septal localization of PlkA. The strain did not have any obvious phenotype suggesting that the C-terminally tagged protein fulfilled its functions at SPBs. We also tried to view localization of GFP–PlkA when expressed from its own promoter, but the GFP signal was under the detection level of our microscopic setup. Nevertheless, the defects observed in the Δ*plkA* deletion mutant (see below) are in perfect agreement with the observed localization pattern for the overexpressed protein.

Journal of Cell Science (2021) 134, jcs256537. doi:10.1242/jcs.256537

Next, we studied the timing of PlkA recruitment to septa. PlkA localized at forming septa as a ring (Fig. 1D), but not as early as Spa10, which localized at the beginning of septation (Fig. S2A). Colocalization of ApsB and PlkA at a near-mature septum revealed that PlkA accumulated at forming septa earlier than ApsB (Fig. S2B). Since Spa10 acts as an anchor for sMTOCs (Zhang et al., 2017), we further checked whether localization of Spa10 was affected by PlkA. Spa10 signals at septa appeared to be normal in a Δ*plkA* mutant (Fig. S2C).

PlkA is involved in polar growth, septation and nuclear distribution

In an early study *plkA* was suggested to be essential (Bachewich et al., 2005), but later it was shown that deletion was not lethal but caused a severe growth phenotype and affected nuclear distribution (Mogilevsky et al., 2012). In this study, we created a Δ*plkA* deletion mutant via homologous recombination and compared the phenotype with *apsB* and *mztA* mutants. Colonies of the Δ*plkA* deletion strain were very small and produced very few conidia, as was described before (Mogilevsky et al., 2012). The growth and sporulation phenotypes were more severe than in the *apsB* or the *mztA* mutants (Fig. S3A, left panel). All phenotypes were rescued by re-introducing an intact copy of the *plkA* open-reading frame (Fig. S3A, right panel). Surprisingly, more septa were observed in hyphae of the Δ*plkA* deletion mutant than in wild type (WT), suggesting a role for PlkA in controlling septation (Fig. 2A). In agreement with this, overexpression of PlkA blocked septation (Bachewich et al., 2005). However, the effect is rather minor, as described before (Mogilevsky et al., 2012), which is in contrast to what is seen in other organisms, like *S. pombe*, where Plo1 is essential for septation (Mulvihill and Hyams, 2002; Tanaka et al., 2001). Nuclear distribution in the Δ*plkA* mutant was abnormal with some anucleate subapical compartments (Fig. 2A). The variation of the number of nuclei in each compartment varied much more than in WT (Fig. 2B).

PlkA colocalizes and interacts with the outer plaque receptor ApsB

Because ApsB was previously shown to play a role in nuclear distribution as well as in astral MT formation (Suelmann et al., 1998; Zhang et al., 2017), and because both proteins localize to MTOCs, we asked whether PlkA interacts with ApsB. First, we tested colocalization of the two proteins. We observed overlapping signals of mCherry–PlkA and GFP–ApsB at SPBs and mature septa both in interphase and during mitosis (Fig. 3A). Using the BiFC system, we tested for protein–protein interaction and detected fluorescent signals at interphase and mitotic SPBs and at mature septa (Fig. 3B). The interaction between PlkA and ApsB was confirmed via yeast two-hybrid (Y2H) analyses with the two combinations AD–PlkA with BD–ApsB, and BD–PlkA with AD–ApsB (Fig. 3C). In addition, we showed self-interaction of ApsB but not of PlkA. Thus, PlkA directly interacts with ApsB, suggesting it functions through regulating ApsB.

Owing to the physical association of PlkA and ApsB, we next asked whether PlkA plays a role in recruiting ApsB to MTOC sites. We introduced GFP–ApsB into a Δ*plkA* deletion strain and compared the GFP signal intensities with those in a corresponding WT strain. GFP–ApsB signals were largely reduced at both SPBs and sMTOCs in the Δ*plkA* strain (Fig. 4A, left panels). Quantification of signal intensities revealed significant reduction of the signals (P<0.0001) to only one-third of that in WT (Fig. 4A, right panel). However, weak ApsB signals were still detected at

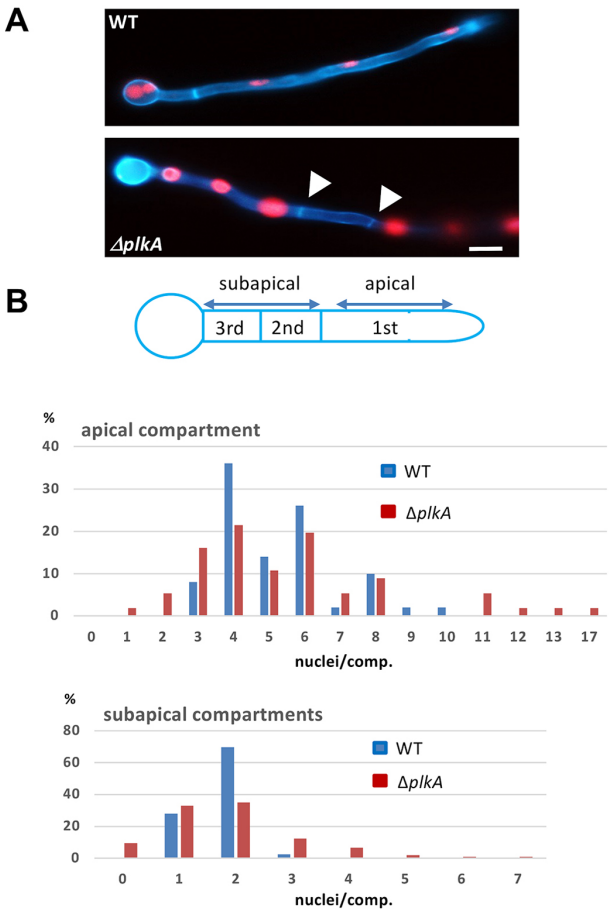

Fig. 2. PlkA is involved in septation and nuclear distribution. (A) Cell walls of WT and a Δ*plkA* deletion strain were stained with Calcofluor White and nuclei visualized through mRFP–H1 expression. Arrowheads indicate two septa of a compartment without any nuclei. (B) Quantification of the percentage of nuclei per compartment in WT and the Δ*plkA* deletion strain in apical (n=50 and 56, respectively) and subapical regions (n=79 and 106) as defined in the scheme.

SPBs and at sMTOCs. The localization of PlkA appeared to be unaffected in the absence of ApsB (Fig. S3B). In the same way, we analyzed the concentration of two further γ-TuRC components, GcpC and MztA. Whereas GcpC is a component of the outer and the inner plaque, MztA is restricted to the inner plaque (Gao et al., 2019). As for ApsB, the concentration of GcpC and MztA at SPBs was largely reduced and, at septa, no signals were observed in the mutant (Fig. 4B,C). Because GcpC and MztA appeared to be absent at sMTOCs in the Δ*plkA* mutant, we analyzed the sMTOC activity by observing the MT emergence from septa. In WT, MTs were nucleated from septa, whereas in the Δ*plkA* mutant no MTs originated from septa, with MTs coming only occasionally from opposite directions (Movies 1 and 2). Hence PlkA improves recruitment of ApsB to both MTOCs and is essential for sMTOC activities. The effect of PlkA on MztA localization suggests that it has an additional role at the inner plaque.

PlkA interacts with the inner plaque receptor PcpA

In order to investigate a role of PlkA at the inner plaque of SPBs, we first examined colocalization of PlkA and PcpA. Expressing the

Journal of Cell Science (2021) 134, jcs256537. doi:10.1242/jcs.256537

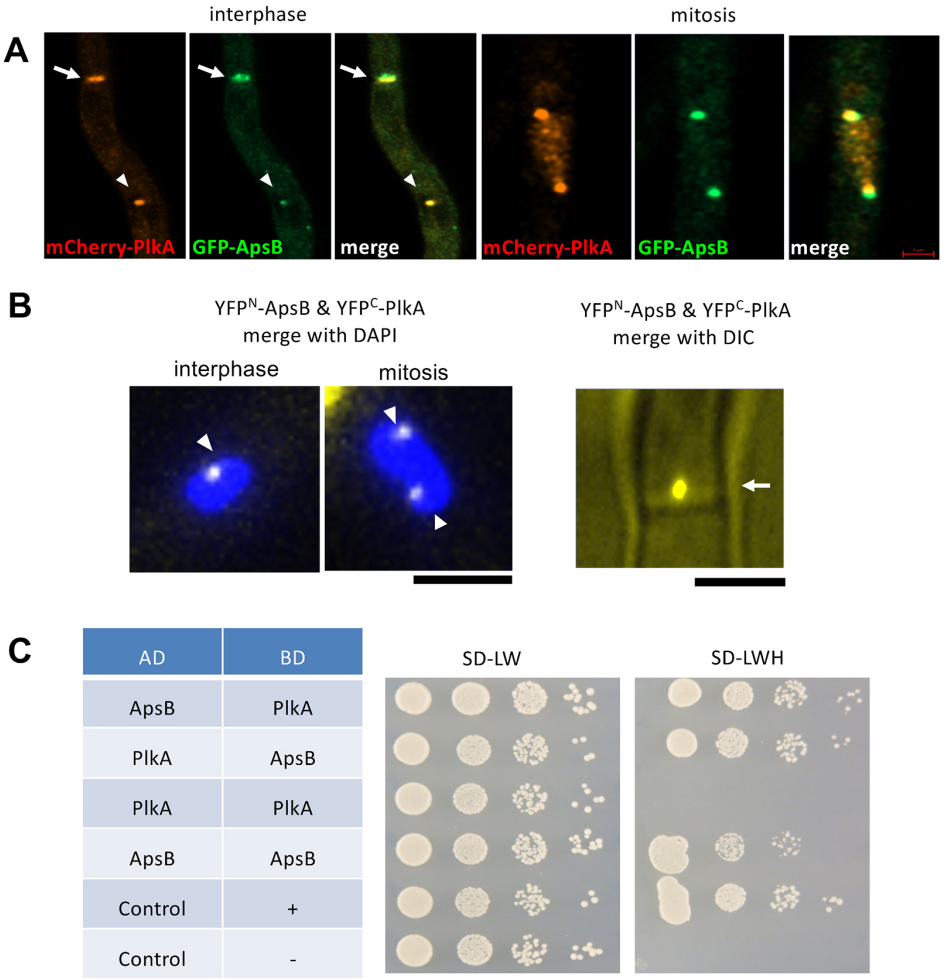

Fig. 3. PlkA colocalizes and interacts with the outer plaque receptor ApsB. (A) PlkA colocalizes with ApsB at sMTOCs and SPBs both in interphase and during mitosis. Strain SXL174 [*alcA(p)::GFP::apsB; alcA(p)::mCherry::plkA*] was incubated in MM (2% glycerol) at 28°C overnight. Arrows indicate septum positions and arrowheads indicate SPB positions. Pictures were taken with the LSM 980 Airyscan microscope. Scale bar: 1 µm. (B) PlkA interacts with ApsB at SPB and sMTOCs revealed with bimolecular fluorescence complementation (BiFC). Strain SXL124 [*alcA(p)::YFP^{N}::apsB; alcA(p)::YFP^{C}::plkA*] was incubated in MM (2% glycerol) at 28°C overnight and imaged. Nuclei were stained with DAPI. Arrowheads indicate YFP signals at SPBs and the arrow points to the YFP signal at a sMTOC. Scale bar: 2 µm. (C) Interaction of PlkA and ApsB confirmed with Y2H *S. cerevisiae* strain Gal4 AD–ApsB with BD–PlkA and AD–PlkA with BD–ApsB. Self-interaction of ApsB and PlkA were investigated with AD–ApsB with BD–ApsB, and AD–PlkA with BD–PlkA strains. Positive and negative controls were included according to the Matchmaker™ Gold yeast two-hybrid system by Clontech. Dilution series of respective strains were grown on SD−LW (selective dropout leucine and tryptophan) and SD−LWH (selective dropout leucine, tryptophan, histidine) agar plates at 30°C for 3 days. Images are representative from three independent experiments.

combination of the two tagged proteins appears to be difficult, because we were unable to generate a stable strain either by transformation or by crossing. Therefore, colocalization could only be observed in a heterokaryon (Fig. 5A). However, the results were confirmed by showing the interaction of the two proteins during interphase and during mitosis in the BiFC assay (Fig. 5B). For the combination of MztA and PlkA, no positive signals were observed (data not shown). PcpA, together with its orthologs (Spc110 in budding yeast and Pcp1 in fission yeast), belongs to the SPM-CM1-PACT receptor family (Chen et al., 2012; Lin et al., 2014; Zhang et al., 2017). The N-terminal SPM-CM1 motif defines the γ-TuRC-interacting motif, and the C-terminal PACT domain defines a MTOC-targeting motif. The central coiled-coil region of PcpA is composed of the Smc domain, which is involved in cell cycle control, cell division and chromosome partitioning. Y2H assays revealed that PlkA interacts with the Smc domain of PcpA in the one combination of AD–PcpA-Smc with BD-PlkA. The other combination, AD–PlkA with BD–PcpA-Smc was negative, and did not result in yeast growth, which could be due to mis-folding of the proteins. No interaction was detected between GcpC and PlkA (Fig. 5C).

PlkA is required for mitotic progression and acts by affecting chromosome condensation

Since PlkA interacted with both receptor proteins ApsB and PcpA, we studied a role in mitosis progression and chromosome segregation. Initial experiments had already shown that *plkA* deletion does have some effect on mitotic progression (Bachewich et al., 2005; Mogilevsky et al., 2012). Therefore, we aimed at analyzing the effect by high-resolution microscopy, and labeled

Journal of Cell Science (2021) 134, jcs256537. doi:10.1242/jcs.256537

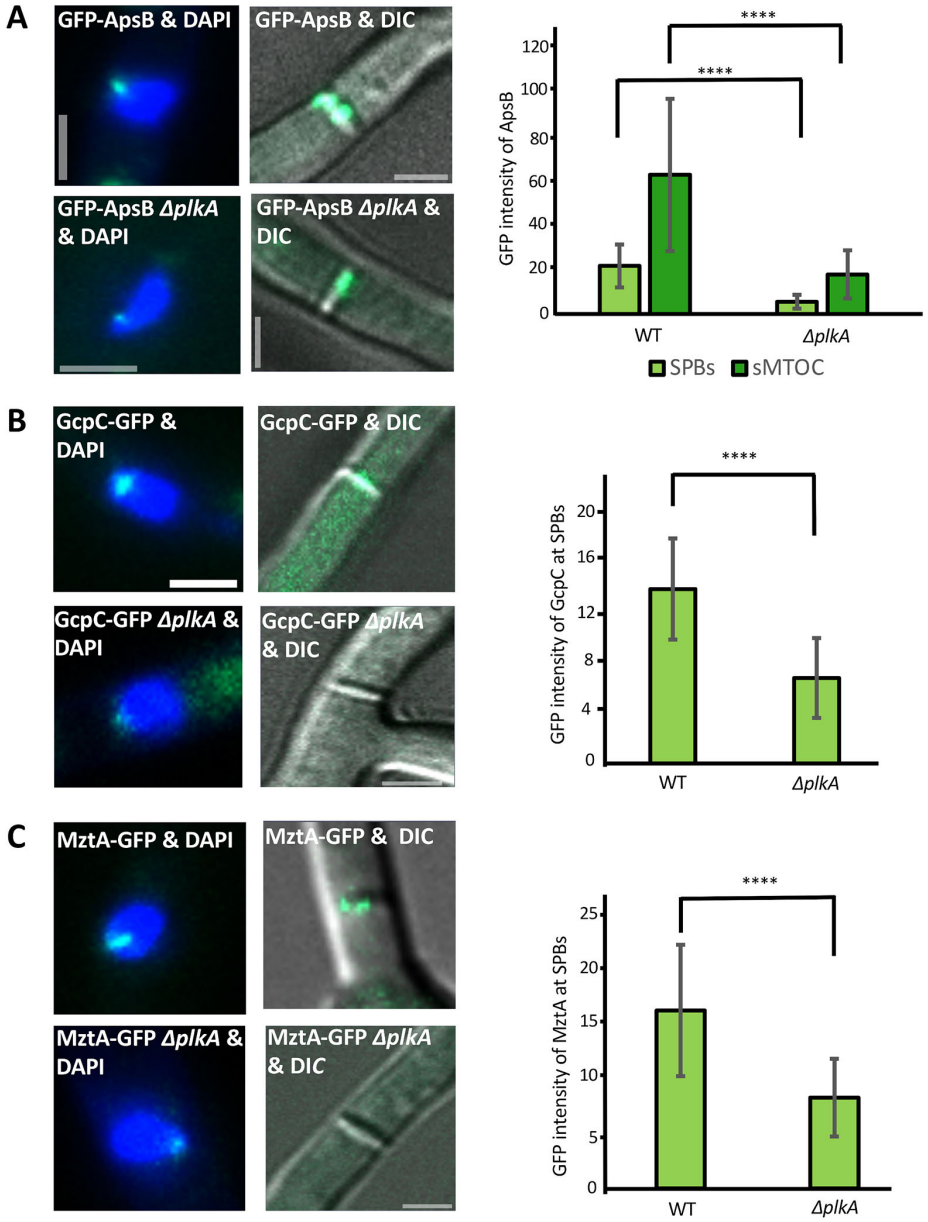

Fig. 4. ApsB, GcpC and MztA localization to SPBs and sMTOCs depend on PlkA. (A) Analysis of the role of PlkA for ApsB recruitment to SPBs and sMTOCs. Strains SYZ2 [*alcA(p)::GFP::apsB*] and SXL135 [Δ*plkA*; *alcA(p)::GFP::apsB*] were incubated in MM (2% glycerol) at 28°C overnight and imaged. Nuclei were stained with DAPI. Scale bars: 2 µm. Images of 10–15 sections were taken along the *Z*-axis at 0.25-µm increments. Maximum projection images were obtained and maximum fluorescence intensities over the background were used for statistical analysis. The exposure time and shutter level were kept identical. 40–50 SPBs and 35–40 septa were checked for each strain. (B) Analysis of the role of PlkA for GcpC recruitment to SPBs and sMTOCs. Strains were SNZ-SH84 (*gcpC::GFP*), SXL131 (Δ*plkA*; *gcpC::GFP*). Growth and imaging were performed as in A. No GFP signal was observed at septa in the Δ*plkA* deletion strain. 50–65 SPBs were analyzed for each strain. (C) Analysis of the role of PlkA for MztA recruitment. Strains were SMS4 (*mztA::GFP*) and SXL129 (Δ*plkA*; *mztA::GFP*). Growth and imaging were performed as in A. At septa no GFP signal was observed in the Δ*plkA* deletion strain. 41–47 SPBs were analyzed. Error bars show the s.d. *****P*<0.0001 compared to WT (Mann–Whitney U test was performed with GraphPad Prism 8).

MTs with GFP–TubA and the chromosomes with mRFP–H1 (histone) in WT and the Δ*plkA* deletion strain to simultaneously visualize mitotic spindles and chromosomes. Time-lapse analyses of mitosis revealed that mitosis was delayed in the mutant as compared to WT, and chromosomes appeared to take longer to condense early during mitosis (Fig. 6A; Movies 3 and 4). We also noticed that the GFP signal intensity in mitotic spindles in the Δ*plkA* deletion strain is reduced in comparison to that in WT (Fig. 6B). PlkA appears to be involved in ensuring adequate numbers of spindle MTs, probably through interacting with PcpA. However, MT numbers may also be determined by other MT dynamics parameters (Szewczyk and Oakley, 2011). However, we did not find significant differences in the polymerization, pausing or depolymerization kinetics between WT and mutant (Fig. 6C,D; Movies 5 and 6).

Kinase activity of PlkA is required for recruitment of ApsB to MTOC sites and astral MT formation but not for spindle morphology

Since PlkA interacts and helps to recruit ApsB to SPBs and sMTOCs, we further asked whether recruitment of ApsB requires the kinase activity of PlkA. To achieve this, we generated a kinase-dead form of PlkA by mutating a conserved catalytic lysine 95 (K) to arginine (R) which should render the protein inactive ($PlkA^{95K/R}$; Fig. 7A) (Berlanga et al., 1998). Whether the modified protein lacks all kinase activity, or whether the activity is only reduced, was not tested. Endogenous PlkA was N-terminally labeled with mCherry and the mutation introduced by homologous integration. mCherry allowed us to analyze the localization of the mutated protein. $PlkA^{95K/R}$ localization at SPBs and sMTOCs appeared not to be affected by the point mutation (Fig. 7B, left),

Journal of Cell Science (2021) 134, jcs256537. doi:10.1242/jcs.256537

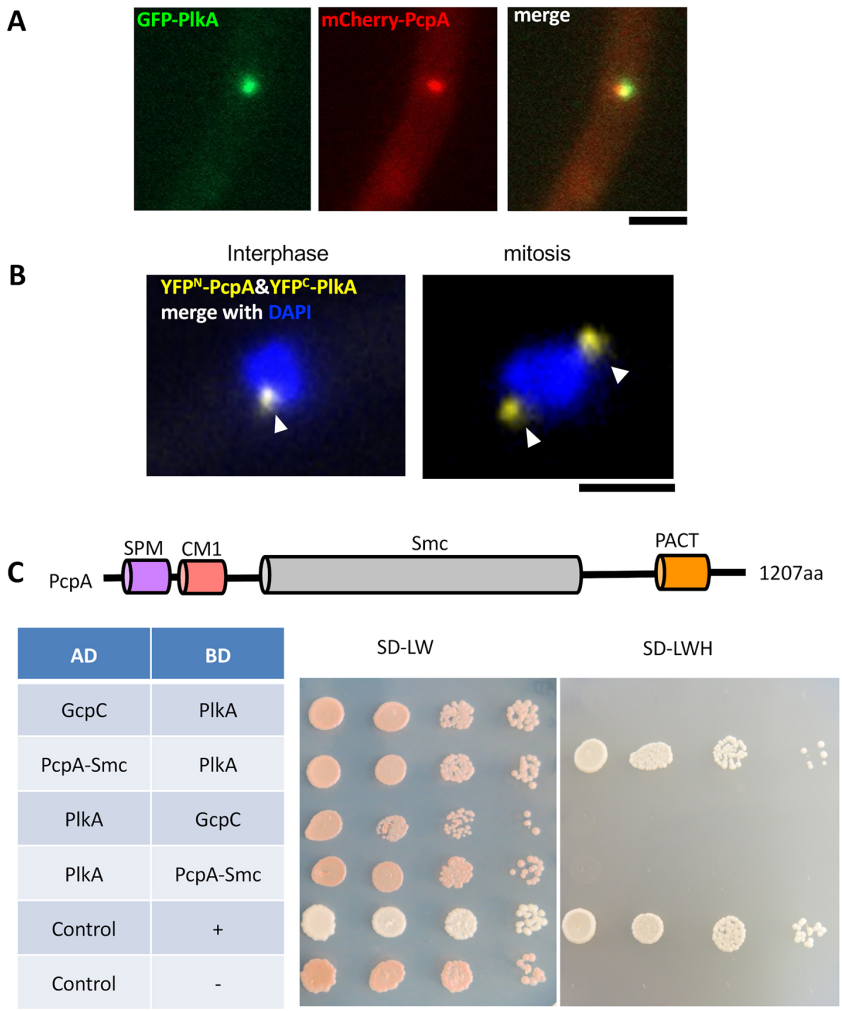

Fig. 5. PlkA interacts with the inner plaque receptor PcpA. (A) PlkA colocalizes with PcpA at SPBs. Strain SSH172 [*alcA(p)::GFP::plkA; alcA(p)::mCherry::pcpA*] is a heterokaryon obtained after the fusion of strains SXL137 and SXL80. Scale bar: 2 µm. (B) Interaction analysis of PlkA and PcpA using bimolecular fluorescence complementation (BiFC). Strain SXW7 [*alcA(p)::YFP^{N}::pcpA; alcA(p)::YFP^{C}::plkA*] was incubated in MM (2% glycerol) at 28°C overnight and imaged. Nuclei were stained with DAPI. The arrowheads mark the SPB positions during interphase and mitosis. Scale bar: 2 µm. (C) Interaction of PlkA and PcpA confirmed with Y2H analysis. The domains of the protein are indicated in the scheme above the experimental data. The Smc domain was analyzed in the Y2H. *S. cerevisiae* strain Gal4 AD–PcpA^{Smc} with BD-PlkA showed positive interaction while neither AD–GcpC with BD–PlkA nor AD–PlkA with BD–GcpC were positive. Positive and negative controls were included according to the Matchmaker™ Gold Yeast Two-Hybrid System by Clontech. Dilution series of respective strains were grown on SD–LW (selective dropout leucine and tryptophan) and SD-LWH (selective dropout leucine, tryptophan, histidine) agar plates at 30°C for 3 days. Images are representative from three independent experiments.

indicating that the kinase activity is not required for correct localization. This is consistent with the notion that localization of polo-like kinases can be attributed to the PBD domain. We then introduced GFP–ApsB into mCherry–PlkA$^{95K/R}$ and compared the signal intensities with those of the WT mCherry–PlkA. In mitotic spindles, we observed an obvious reduction of GFP–ApsB signals at both spindle poles in the catalytic mutant (Fig. 7B, right). GFP–ApsB signals at septa and at SPBs were also reduced during interphase (Fig. S4A).

In WT, mitotic spindles are very compact and condensed during metaphase, and abnormal spindles are very rare. In our experiment, all spindles appeared normal in wild type (n=152), whereas the deletion mutant showed ~20% and the catalytic mutant ~4% abnormal spindles (defined as thin, fusiform, D-form or curved) (Fig. 7C,D). The spindle morphology phenotype in the Δ*plkA* deletion strain is in agreement with previous findings (Mogilevsky et al., 2012). The fact that the deletion mutant displayed a more-severe phenotype than the catalytic mutant, suggests that there are additional non-catalytic roles of PlkA.

Because ApsB is required for astral MT formation during anaphase, and the fact that PlkA kinase activity supports ApsB recruitment to SPBs, we asked whether the catalytic activity is required for astral MT formation. Nearly 95% of the nuclei in WT nucleated more than three astral MTs at anaphase as compared to 4% in the Δ*plkA* deletion or the catalytic *plkA* mutant strain (Fig. 7E). Thus, we suggest that PlkA regulates astral MT formation via recruiting ApsB to the outer plaques of SPBs in a phosphorylation-dependent manner. Furthermore, PlkA plays additional roles in spindle morphology that are independent of its phosphorylation activity.

PlkA functions as a kinase and as a scaffolding protein

To gain insights of the role of the catalytic activity of PlkA in vegetative growth, we compared the phenotypes of a Δ*plkA* deletion strain with those of the deletion strain expressing mCherry–PlkA or mCherry–PlkA$^{95K/R}$. Both constructs were driven by the *alcA* promoter, which is repressed during growth on glucose and de-repressed during growth on glycerol. Compact colonies were observed with the Δ*plkA* deletion strain and the *plkA*$^{95K/R}$ mutant under repressing conditions (Fig. S4B), indicating that kinase function is important for polar growth. The fact that the deletion mutant displayed a more-severe phenotype shows that the *alcA* promoter is not 100% repressed on agar plates with 2% glucose. However, with the low expression levels, we noticed that sporulation in the *plkA*$^{95K/R}$ mutant colonies appeared higher than that in the Δ*plkA* deletion strain when grown on glucose (Fig. S4B).

Journal of Cell Science (2021) 134, jcs256537. doi:10.1242/jcs.256537

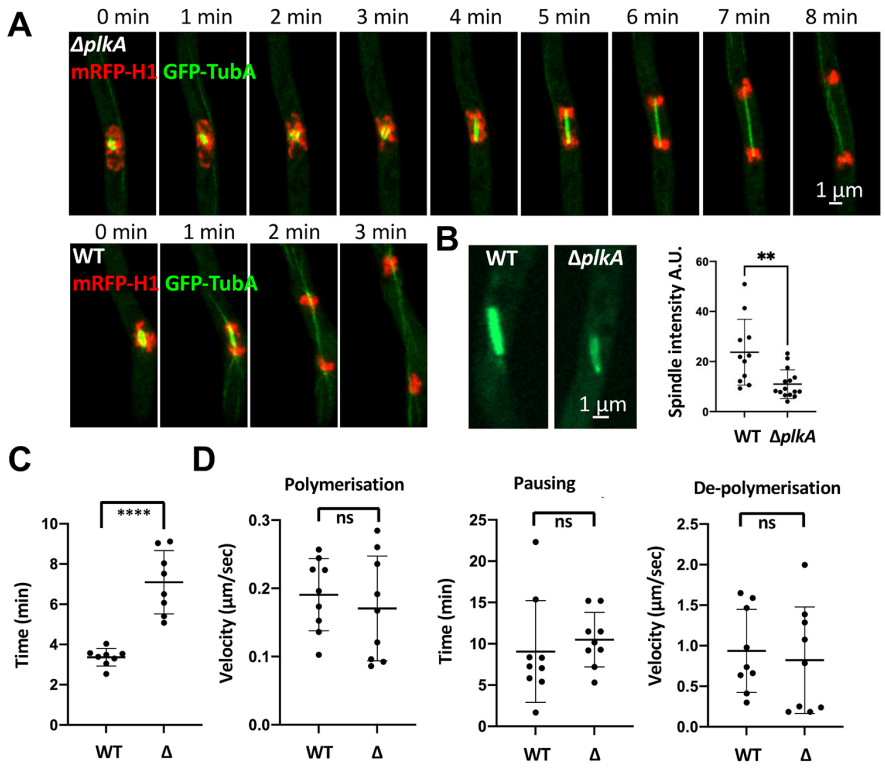

Fig. 6. The role of PlkA in mitosis. (A) Visualization of mitosis in WT and a Δ*plkA* deletion strain using GFP–TubA (green) and mRFP–H1 (red). Pictures were taken with the LSM 980 Airyscan microscope. (B) Quantification (A.U., arbitrary units) of mitotic spindle intensities in WT (n=15) and the Δ*plkA* deletion strain (n=11). Images were taken as *Z*-stack with maximum projection. The intensities of the spindle area were multiplied by the size and the cytosolic background subtracted. Scale bar: 1 µm. (C) The duration of mitotic events was quantified in each strain (n=8). (D) Determination of MT dynamics (n=9) in WT and Δ*plkA* (Δ) strains. Error bars are s.d. **P<0.01; ****P<0.0001; ns, not significant compared to WT (Mann–Whitney U test was performed with GraphPad Prism 8).

Therefore, we quantified the number of conidia produced in each strain (n=16) and found for WT the number was 30×10^6/cm^2, for the *plkA*$^{95K/R}$ mutant this was 41×10^6/cm^2 and this was only 1.8×10^6/cm^2 for the Δ*plkA* deletion strain. These results indicate that there are additional roles of PlkA besides the catalytic kinase activity.

To identify putative interacting partners of PlkA and phosphorylation sites in ApsB, we performed pulldown experiments using the GFP-trap technology followed by mass spectrometry. Western blot analysis of the precipitate showed successful pulldown of endogenous PlkA and ApsB (data not shown). Using mass spectrometry, we found all tubulin proteins. TubA and TubB (α-tubulins), BenA, TubC (β-tubulins) were among the putative binding partners for PlkA (Fig. S5A, Table S1). In combination with the fact that PlkA localizes along mitotic spindles, this may explain the abnormal morphology of spindles in the absence of PlkA.

Mass spectrometry of pulled-down ApsB revealed three phosphorylation sites in two peptides, two of them prior to the CM motif and one at S1414 located in front of the C-terminal MASC domain (Fig. S5). For details for identifying the sites see Figs S5–S7. However, in the Δ*plkA* deletion mutant, those phosphorylated peptides were not detected. Because of the incomplete coverage of ApsB with the identified peptides, currently we cannot exclude there could be additional phosphosites. To gain insights into the function of the phosphorylation sites, we mutated the three serine residues into alanine residues (non-phosphorylatable) or aspartic acid (a phosphomimetic) individually. However, ApsB protein with single changes of either serine to alanine (S/A) or aspartic acid (S/D) rescued all the Δ*apsB* deletion phenotypes (Fig. S8A), and the localization of ApsB to SPBs and sMTOCs appeared not to be affected. We then created an ApsB allele with a triple mutation of the three serine residues to alanine or aspartic acid (denoted AAA or DDD) and introduced it into the Δ*apsB* deletion strain. The sporulation deficiency of the Δ*apsB* deletion strain was not fully rescued indicating that those sites are important for development (Fig. S8B). Mitotic spindle morphology or functioning was not affected in the strains, suggesting additional residues are required in this process (Fig. S8C).

Taken together, we show that PlkA interacts and recruits ApsB in a phosphorylation-dependent manner, which is important for astral MT formation and sMTOC activities. In addition, PlkA interacts with the inner plaque receptor PcpA and mitotic spindles to stabilize the mitotic spindles, which function as a scaffolding unit inside the nuclei.

DISCUSSION

The study of the role of PlkA in MTOC functioning in *A. nidulans* revealed several interesting aspects. Our results suggest that PlkA is involved in the coordination of the activity of SPB outer plaques and septal MTOCs (Fig. 8). In addition, the protein is required at the inner plaque of the SPB. However, unlike what is found in other organisms, PlkA is not essential. This is even more surprising in the light that PlkA is the only polo-like kinase in *A. nidulans*. Besides its catalytic function as a kinase, PlkA appears to fulfill scaffold functions. This could be an ancient function, because the catalytic and the non-catalytic functions appear to have diverged during evolution.

PlkA of *A. nidulans* serves catalytic and non-catalytic functions

We generated a *plkA* gene deletion strain and a strain with a PlkA kinase-dead version. They both were impaired in MT formation from SPB outer plaques and sMTOCs. This can be explained through the action on the receptor protein, ApsB, which needs to be

Journal of Cell Science (2021) 134, jcs256537. doi:10.1242/jcs.256537

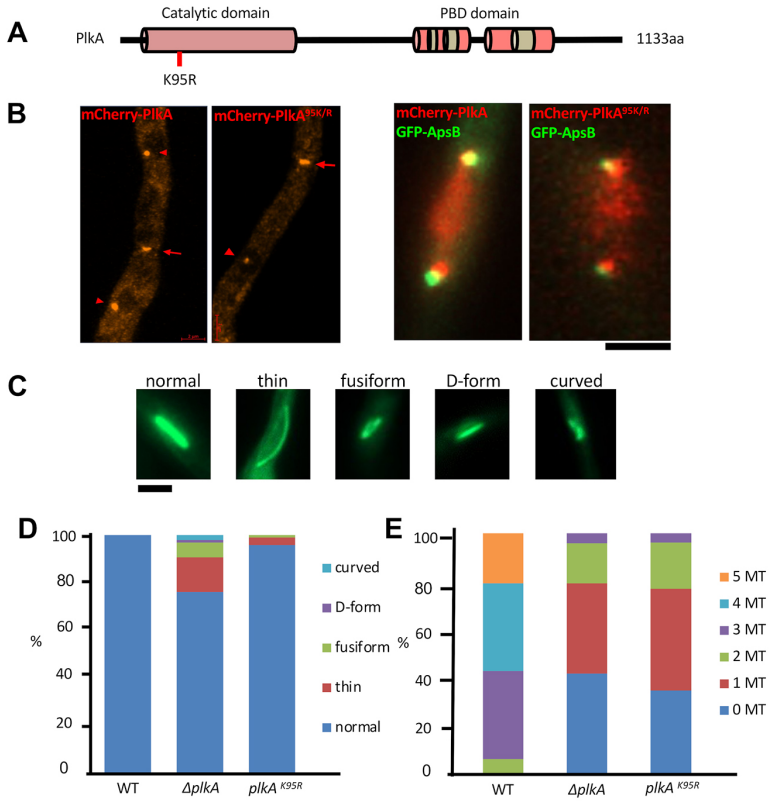

Fig. 7. Effects of the replacement of PlkA lysine 95 with arginine on ApsB recruitment to SPBs, on spindle morphology and on astral MT formation. (A,B) Analysis of the catalytic role of PlkA in ApsB recruitment to MTOCs. (A) Scheme of the domain organization of PlkA and indication of the critical lysine residue 95. (B) Mutation of the catalytic residue PlkA$^{95K/R}$ does not affect PlkA localization but reduces ApsB recruitment to mitotic spindles. Strains SXL158 [*alcA(p)::mCherry::plkA*], SXL159 [*alcA(p)::mCherry::plkA*$^{95K/R}$], SXL174 [*alcA(p)::GFP::apsB; alcA(p)::mCherry::plkA*] and SXL175 [*alcA(p)::GFP::apsB; alcA(p)::mCherry::plkA*$^{95K/R}$] were incubated in MM (2% glycerol) at 28°C overnight and imaged. Left, the arrows indicate the positions of septa and the arrowheads indicate the positions of SPBs. Right, merged images of mCherry-PlkA with GFP-ApsB and mCherry^{95R} with GFP-ApsB at the mitotic SPBs. Pictures were taken with the LSM 980 Airyscan microscope. Images are representative from at least three independent experiments. Scale bar: 2 µm. (C) Shape of mitotic spindles in WT, the Δ*plkA* deletion and the catalytic mutant. Strains SJW65 [*alcA(p)::GFP::tuba*], SXL177 [Δ*plkA, alcA(p)::GFP::tuba*] and SXL178 [*alcA(p)::GFP::tubA; alcA(p)::mCherry::plkA*$^{95K/R}$] were grown in 8-well u-slides at 28°C overnight. Scale bar: 2 µm. (D) Quantification of the spindle shapes. 152 spindles in WT, 74 spindles in the Δ*plkA* deletion and 92 spindles in the *plkA*^{K95R} mutant strain were counted. (E) Quantification of astral MTs. The same strains as in C were grown in 8-well u-slides at 28°C overnight. 19 anaphase spindles in WT, 24 in the Δ*plkA*-deletion and 26 in the *plkA*^{K95R}-mutant strain were analyzed.

phosphorylated by PlkA in order to recruit the γ-TuSC to the outer plaque of the SPB and the γ-TuRCs to the sMTOCs (Fig. 8). PlkA appears to be dispensable for mitotic spindle formation. However, whereas spindle morphology was affected in the Δ*plkA* deletion mutant, it was normal in the kinase-dead mutant strain. Given the fact that PlkA interacts with the inner plaque receptor PcpA, it might facilitate the recruitment of γ-TuRCs to inner plaques, thereby ensuring adequate numbers of spindle MTs during mitosis (Fig. 8). In addition, PlkA localized inside the mitotic spindle and interacted with tubulins (Fig. 1B; Fig. S5A). This could be important for proper spindle formation and morphology. We noticed that without PlkA, chromosomes did not condense as fast as in WT. However, further studies are required to unravel the specific function of PlkA in this process. The localization and functioning of PlkA at septal MTOCs define a novel function for a polo-like kinase at non-centrosomal MTOCs. Thus, we propose that PlkA in *A. nidulans* plays dual roles as a kinase at the outer plaques of SPBs and sMTOCs, and as a scaffolding protein inside mitotic nuclei (Fig. 8). There is already some evidence for non-catalytic roles for Plk2, Plk4 and Plk5. In human, Plk5 is an inactive kinase and Plk2 has synaptic functions that are independent of its kinase activity (de Cárcer et al., 2011; Evers et al., 2010). Furthermore, *Caenorhabditis elegans* ZYG-1 (the homolog of Plk4) has been shown to have a kinase-independent function in SAS-6 recruitment to the mother centriole (Lettman et al., 2013). *A. nidulans* PlkA hence could be an ancient protein combining the function of several Plks, which were separated during evolution to different proteins. Likewise, phylogenetic analysis placed PlkA closest to Plk4 (Mogilevsky et al., 2012).

There is a second line of evidence that PlkA serves functions independently of the kinase activity. We observed that a kinase-dead version of PlkA was sufficient to allow sporulation, whereas in the absence of PlkA sporulation was strongly impaired. The exact role of the PlkA protein during sporulation presently remains unknown.

The next question concerns the targeting mechanism of PlkA. In Cdc5/Plk1 the Polo box domain (PBD) domain, specifically a phosphopeptide-binding motif inside the PBD domain, is essential for subcellular localization and function (Lee et al., 1998; Song et al., 2000). The PBD domain binds to a phosphopeptide in a so-called priming substrate (Elia et al., 2003). In addition, the PBD domain in Plk1 regulates its kinase activity via an auto-inhibitory mechanism (Cheng et al., 2003; Jang et al., 2002). Although the PBD domain of *A. nidulans* PlkA is divergent from Plk1, it contains the conserved residues that are important for phospho-peptide recognition (Mogilevsky et al., 2012). Other studies have revealed that Plk1 can bind also to unphosphorylated substrates (García-Álvarez et al., 2007). Therefore, it is possible that both the phospho-peptide recognition mechanism and another binding mechanism regulate PlkA localization. Although, the priming substrate and its upstream kinase are not known yet for PlkA, we can exclude ApsB as the priming substrate, because PlkA also localized to MTOCs in the absence of ApsB.

The conserved and divergent roles of PlkA compared to other Plk1 proteins

In this study, we present evidence that PlkA binds and either indirectly or directly phosphorylates the γ-TuCR protein ApsB at the outer plaque of SPBs and sMTOCs, which are essential for astral MT (mitosis) and septal MT (interphase) nucleation. In addition, PlkA binds to the inner plaque receptor PcpA, which is indispensable for mitotic spindle assembly. In humans, Plk1 is essential for driving centrosome maturation through phosphorylating the PCM protein pericentrin during mitosis (Lee and Rhee, 2011).

Journal of Cell Science (2021) 134, jcs256537. doi:10.1242/jcs.256537

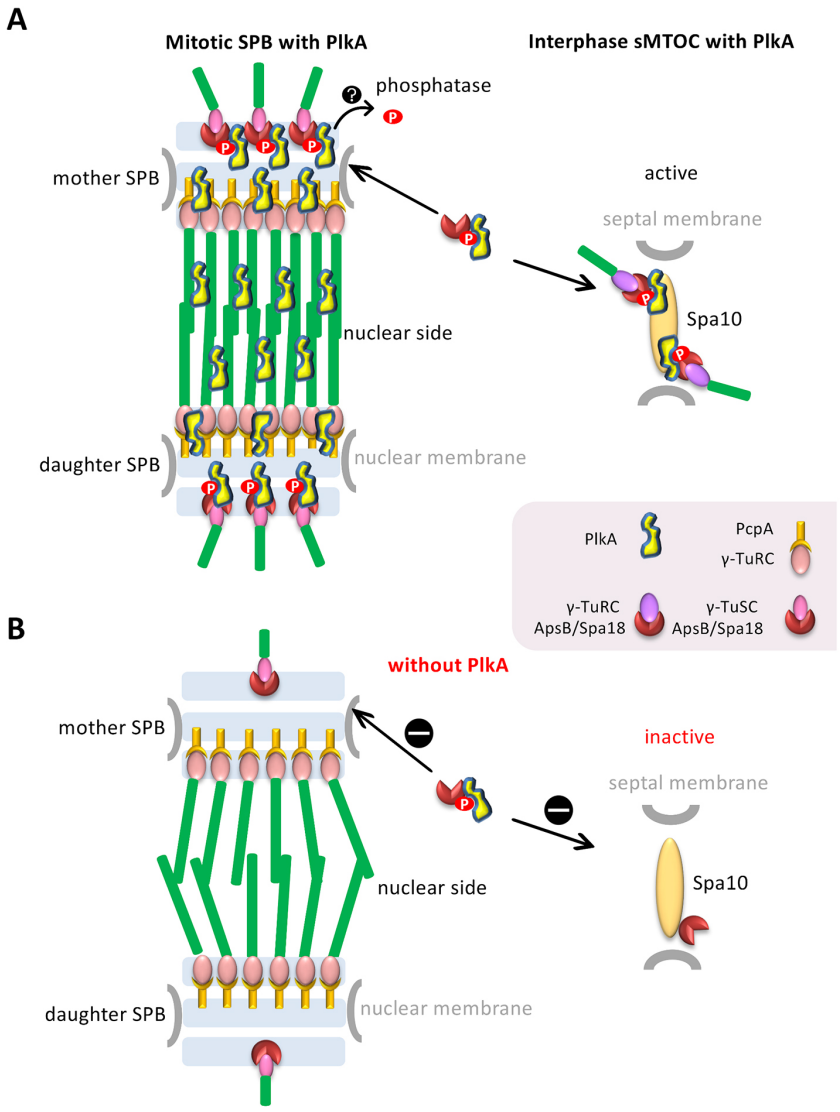

Fig. 8. Proposed model of PlkA in regulating mitotic SPBs and sMTOC activities in *A. nidulans*. PlkA coordinates the activity of SPB outer plaques and the sMTOC activity via phosphorylating and recruiting ApsB, thus promoting astral and septal MT formation. PlkA also binds to PcpA at SPB inner plaques and interacts with spindle microtubules as a scaffolding unit. For further explanation, see the Discussion.

Similarly, in *D. melanogaster*, Polo (the Plk1 homolog) initiates the phosphorylation-dependent assembly of a Cnn (the CDK5RAP2 homolog) scaffold that is essential for centrosome maturation (Conduit et al., 2014). *A. nidulans* PlkA shares its roles in phosphorylating PCM-related components at centrosomes/SPBs to increase MT formation with metazoan Plk1. However, at the inner plaque, it only binds to PcpA and guarantees morphologically and functionally normal mitotic spindles, probably without phosphorylation of the binding partner. Mitotic spindles, although often misshapen and probably containing less MTs than in WT, were produced in the PlkA kinase-dead and in the Δ*plkA* deletion strain. Furthermore, we present a novel function for the polo-like kinase PlkA in regulating non-centrosomal MTOC activities.

Another difference concerns the essential roles of other Plk1 orthologs for mitotic entry and cytokinesis. In *S. cerevisiae* and in *S. pombe*, Cdc5/Plo1 function as essential upstream regulators of the MEN network and the SIN networks (Song and Lee, 2001; Tanaka et al., 2001). Both, mitotic entry and cytokinesis appear to occur in the Δ*plkA* deletion strain. By contrast, NIMA kinase in *A. nidulans* is essential for mitotic entry and its degradation is required for mitotic exit (Osmani et al., 1991; Pu and Osmani, 1995)

Although Plks are traditionally implicated in cell cycle progression, there is increasing evidence for roles of Plks outside cell division, especially for Polo, Plk2 and Plk3 functioning in meiosis, asymmetric cell fate determination and synaptic plasticity (Archambault and Glover, 2009). As mentioned before, the *A. nidulans* PlkA sequence is related to that of Plk4. Plk4 plays a role in centriole-independent MTOC formation, and promotes MT nucleation in the acentriolar mouse embryo (Coelho et al., 2013). The non-centrosomal functions of PlkA may be attributed to this similarity with Plk4.

MATERIALS AND METHODS

Strains, plasmids and culture conditions

Supplemented minimal (MM) and complete medium (YAG) for *A. nidulans* were prepared as previously described, and standard strain construction procedures were used (Hill and Käfer, 2001). Expression of tagged genes

under the control of the *alcA* promoter was regulated by the carbon source with repression on 2% glucose and de-repression on glycerol (2%) (Waring et al., 1989). Lists of *A. nidulans* strains and yeast strains used in this study are given in Tables S2 and S3. Standard laboratory *Escherichia coli* strains (Top 10 F′) were used. Plasmids are listed in Table S4.

Molecular techniques

Standard DNA transformation procedures were used for *A. nidulans* (Yelton et al., 1984) and *Escherichia coli* (Sambrook and Russel, 1999). For PCR experiments, standard protocols were applied using a Biometra Personal Cycler (Biometra, Göttingen, Germany) for the reaction cycles. Phusion polymerase was used (expressed in *E. coli* and purified). Denaturation was achieved at 98°C, annealing temperatures were chosen according to the corresponding DNA oligonucleotides, and the polymerization temperature was 72°C. All DNA oligonucleotides used in this study are listed in Table S5. DNA sequencing was performed commercially (MWG Biotech, Ebersberg, Germany). Total DNA was extracted from *A. nidulans* according to Zekert et al. (2010).

Construction of the Δ*plkA* deletion strain and re-complementation

The Δ*plkA* deletion strain was created by protoplast transformation and homologous integration of a fusion PCR-derived knockout cassette. The flanking regions of *plkA* were amplified by PCR with genomic DNA as template. Primer pair plkA-LB_fwd/plkA-LB-pyroA linker_rev (Table S5) was used for the upstream region of *plkA* and plkA-RB-pyroA linker_fwd/plkA-RB_rev for the downstream region. *pyroA* was amplified with pyroA_fwd/pyroA_rev. Then the left border (LB), *pyroA* and right border (RB) were fused together by fusion PCR with nested primers plkA-LB-N_fwd and plkA-RB-N_rev. The construct was ligated into pJET1.2/blunt, yielding vector pXL79. After transformation of pXL79 to TN02A3 and selection by diagnostic PCR (Table S5; primers, plkA-dele_check_fwd/plkA-RB_rev), the Δ*plkA* deletion strain SXL122 was selected.

For re-complementation, we constructed a plasmid with the whole open reading frame of *plkA* and an auxotrophic marker *AfpyrG* and introduced it into the deletion mutant. The natural promoter of *plkA*, open reading frame (ORF), terminator and full-length *AfpyrG* was fused into pJET with NEBuilder HiFi DNA Assembly Master Mix (NEB) in one step. The ORF of *plkA* was amplified using primers:plkA-promo_builder_fwd/plkA-termi_pyrG linker_rev; and *AfpyrG* was amplified using primers pyrG_fwd/pyrG builder_rev. The two fragments were ligated to pJET1.2/blunt resulting in plasmid pXL81. After transformation into the Δ*plkA* deletion strain SXL122, all phenotypes were rescued (SXL126).

Protein tagging in the Δ*plkA* deletion strain

To check ApsB localization in a Δ*plkA* deletion strain, we crossed the two strains SXL122 (Δ*plkA*) and SYZ2 (GFP–ApsB) (Todd et al., 2007). After microscopic and phenotypic screening, the recombinant strain SXL135 was selected. For checking GcpC and MztA localization in the absence of PlkA, we introduced a C-terminal tagging cassette of GcpC/MztA into the Δ*plkA* deletion strain, resulting in strains SXL129 (Δ*plkA*; *mztA-GFP*) and SXL131 (Δ*plkA*; *gcpC-GFP*). The homologous integration events of GcpC and MztA were confirmed with primers pyrG check_fwd/gcpC C-termi check_rev and pyrG check_fwd/mztA C-termi check_rev (Table S5).

C-terminal tagging of PlkA with GFP under natural promoter control

PlkA was tagged with GFP at the C-terminus expressed from the natural promoter. A 1 kb region from the 3′-end of the *plkA* gene was amplified with the primer pair PlkA-C-termi_fwd/PlkA-C-termi_GA linker_rev, and 1 kb of the terminator region of the gene was amplified with the primer pair PlkA-RB-pyrG linker_fwd/PlkA-RB_rev. The fragment of a *GFP::pyrG* cassette was amplified from pFNO3 (Yang et al., 2004) using primers GA linker_fwd/pyrG overhang_rev. Subsequently, the three fragments were fused together by fusion PCR with nested primers PlkA-C-termi-N_fwd/PlkA-RB-N_rev (Table S5). The construct was ligated to pJET1.2/blunt, resulting in plasmid pXL82 (Table S4). The plasmid was transformed into TN02A3, and the strain SXL137 (Table S2), in which the construct had replaced the endogenous 3′-end of the gene, was checked with primers pyrG check fwd/PlkA C-termi check rev. The strain expresses PlkA–GFP from the natural promoter and PlkA–GFP is the only source of PlkA.

N-terminal tagging of PlkA with mCherry under the control of the *alcA* promoter

Besides C-terminal tagging with GFP, we also created two N-terminally tagged strains. PlkA was fused with either GFP or mCherry at the N-terminus under *alcA* promoter control. N-terminally, 1.0 kb of *plkA* starting from the start codon was amplified with primers plkA_AscI_fwd and plkA 1kb_PacI_rev (*Asc*I and *Pac*I restriction sites are used and are in italics in Table S5), cloned into the pMCB17apx vector, resulting in pXL83 (*alcA-mCherry-plkA*) and pXL84 (*alcA-GFP-plkA*) (Table S4). The plasmids were subsequently transformed into TN02A3. After homologous recombination, this yields the N-terminally fused protein expressed under the control of the *alcA* promoter and a truncated 5′-end fused to the natural promoter. The resulting strains are SXL158 (mCherry–PlkA) and SXL164 (GFP–PlkA) (Table S2). Using primers alcA check_fwd/PlkA 1 kb Int check_rev (outside of the 1 kb ORF), homologous recombination was confirmed.

Colocalization of two proteins with GFP and mCherry

To observe the sMTOC activities during mitosis, we created a strain in which the MT plus-end tracking protein KipA was tagged with GFP while mitotic spindles were labeled with mCherry. The plasmid PSK82 *pMCB17apx-GFP-kipA* was transformed into strain SSH127 (mCherry-tubA) resulting in strain SXW1.

To investigate colocalization of PlkA with ApsB, strain SYZ2 (GFP–ApsB) was crossed with strain SXL158 (mCherry–PlkA) according to protocol from Todd et al. (2007). After microscopic screening, the recombinant strain SXL174 was selected.

To investigate the timing of the recruitment of PlkA at forming septa, it was colocalized with Spa10. PlkA was tagged with mCherry at the N-terminus in a strain where Spa10 was C-terminally tagged with GFP. Strain SXL158 (mCherry-PlkA) was crossed with SRM212 (Spa10-GFP) yielding strain SXL179.

To investigate colocalization of PlkA and α-tubulin TubA, the N-terminal tagging plasmid of PlkA was introduced into the GFP–TubA strain. The plasmid pXL83 pMCB17apx-mCherry-*plkA* was transformed into strain 65 resulting in strain SXL176. The homologous integration event for PlkA was confirmed with primers alcA check_fwd/plkA 1 kb Int check_rev (Table S5).

To investigate simultaneous localization of chromosomes and tubulin, we created a strain (SSH167) harboring mRFP–H1 and GFP–TubA by crossing CDS445 (kindly provided by Steven Osmani, Ohio State University, OH, USA) with SJW65. SSH167 was also crossed to SXL122 (Δ*plkA*) to generate strain SSH169, which harbors mRFP–H1 and GFP–TubA in a Δ*plkA* background.

Generation of a GFP-labeled MT strain with a temperature-sensitive block in mitosis

To block the cells in mitosis, we combined a temperature-sensitive mutation *bimE7* with GFP labeling of TubA. The original *bimE7* mutant SO4 was crossed with SJW02, and, after temperature screening and microscopic analysis, the recombinant strain SXL136 was selected. The resulting strain allowed us to block the hyphae in mitosis at restrictive temperature of 42°C and monitor sMTOC activities.

Bimolecular fluorescence complementation assay

To analyze the interaction of PlkA with ApsB and PlkA with PcpA, a bimolecular fluorescence complementation assay (BiFC or Split YFP) was performed. In these analyses, PlkA was tagged with YFP^C at the N-terminus under the control of the *alcA* promoter while ApsB or PcpA were tagged with YFP^N at the N-terminus. Similar to the generation of the GFP-tagging plasmid, 1 kb of *plkA* was amplified with primers plkA_AscI_fwd and plkA_PacI_rev, and was cloned into the pMCB17apx-YFP^C vector, which

contained YFP^C instead of *GFP*, yielding pXW8. The N-terminal YFP^N tagging plasmid of ApsB (pYZ59) and PcpA (pXL58) were created previously. Then pXW8 and pYZ59 were co-transformed into TN02A3; pXW8 and pXL58 were co-transformed into TN02A3 as well. After screening, the resulting strains SXL124 and SXL125 were examined for YFP signals. All the YFP strains were checked for homologous integration events by PCR.

Yeast two-hybrid assay

The Matchmaker™ Gold Yeast Two-Hybrid System (Clontech Laboratories, Inc.) was used in this work following the user manual. Full-length *plkA* and *gcpC* cDNA fragments were amplified by annealing three or two coding sequences (CDS) together with genomic (g)DNA as template due to the large size of cDNAs. Primer pair plkA-CDS1_builder_fwd/plkA-CDS1_CDS2 linker_rev was used for amplifying PlkA CDS1, primer pair plkA-CDS2_fwd/plkA-CDS2_rev for PlkA CDS2 and primer pair plkA-CDS3_CDS2 linker_fwd/plkA-CDS3_builder_rev for PlkA CDS3. Then the three CDS were fused into pJET with NEBuilder HiFi DNA Assembly Master Mix (NEB) in a one-step ligation. The resulting plasmid is pXL102 with the *plkA* exon in pJET. Then primer pair plkA *Nde*I AD/BD_fwd/plkA *Xma*I AD/BD_rev was used for amplifying from pXL102 as cDNA template. After digestion of the PCR products with *Nde*I and *Xma*I restriction enzymes, and respective ligation into digested pGBKT7 and pGADT7-Rec, two plasmids pXL111 (BD–PlkA) and pXL112 (AD–PlkA) were generated. GcpC plasmids were created similarly, resulting in plasmid pJA5 (AD–GcpC) and pJA6 (BD–GcpC). Primer pair $pcpA^{Smc}$_*Nde*I AD/BD_fwd/$pcpA^{Smc}$_ *Xma*I AD/BD_rev was used to amplify Smc domain of PcpA with gDNA as template. After digestion, the PCR product was ligated into digested pGBKT7 and pGADT7-Rec, resulting in two plasmids pXL125 (AD-$PcpA^{Smc}$), pXL126 (BD-$PcpA^{Smc}$). The yeast strain AH109 was used for transformation of the AD vectors and strain Y187 was used for transformation of the BD vectors. The lithium chloride method was used for transformation and transformants were selected on selective synthetic dropout medium as described in the Matchmaker™ GAL4 two-hybrid system manual. The resulting transformed strains of AH109 and Y187 were then mated yielding Y2H strains used for interaction detection. All Y2H strains are listed in Table S3. To analyze the interaction of the proteins, a 5 ml overnight culture of Y2H strain in SD medium was incubated overnight at 30°C at 230 rpm. The culture was diluted to an optical density at 600 nm (OD_{600}) of 1, as well as a dilution series (1:10, 1:100, 1:1000). Then 5 µl of each suspension (1:1–1:1000) was dropped onto the SD−LW and SD−LWH agar plates respectively with positive and negative controls. We exclude the possibility of self-activation in BD or AD vector alone via the negative interaction result between GcpC and PlkA.

Modification of specific amino acids in PlkA and ApsB by site-directed mutagenesis

To generate a kinase-dead form of PlkA, the Q5 site-directed mutagenesis kit was used for mutating lysine 95 (K) to arginine (R) by designing a mutagenesis primer pair. Primer pair plkA_95K/R_fwd/plkA_95K/R_rev was designed with NEBase Changer tool including the annealing temperature. The template plasmid used was pXL83 (*alcA-mCherry-plkA*). Following the procedures in the kit, the mutated plasmid was sequenced to make sure only the targeted base pairs were mutated using primer plkA_95 seq_fwd (Table S5). The resulting plasmid was pXL114. After transformation into TN02A3, the resulting strain SXL159 (Table S2), harboring the homologous integration and mutated site, was selected after sequencing.

To generate the single mutation of ApsB phosphorylation sites, the same method was applied. The used primer pairs designed with NEBase Changer tool are apsB-321S/A_fwd/apsB-321S/A_rev; apsB-327S/A_fwd/apsB-327S/A_rev and apsB-1414S/A_fwd/apsB-1414S/A_rev for mutating serine sites at 321, 327 and 1414 to alanine, respectively. Primer pairs apsB-321S/D_fwd/apsB-321S/D_rev, apsB-327S/D_fwd/apsB-327S/D_rev and apsB-1414S/D_fwd/apsB-1414S/D_rev were used for mutating the three sites to aspartic acid, respectively (Table S5). The used template plasmid was pXL106. After sequencing with primers apsB-321,327 seq_fwd and apsB-1414 seq_fwd, the resulting plasmids which harbor the respective single mutation and maintain the integrity of ORF are pXL107(1414A), pXL108(1414D), pXL109(321A), pXL110(321D), pXL117(327A) and pXL118(327D). Then the plasmids were transformed into Δ*apsB* deletion strain, resulting in strains SXL160, SXL161, SXL162, SXL163, SXL168 and SXL169, respectively (Table S2).

To generate the triple mutation of ApsB phosphorylation sites, a second round of site-directed mutagenesis was performed based on the 1414-site mutation plasmids. Primer pair apsB-321S/A,327S/A_fwd/apsB-321S/A,327S/A_rev was used for mutating both the 321 and 327 sites into alanine at the same time. Plasmid pXL107 was used as template. Primer pair apsB-321S/D,327S/D_fwd/apsB-321S/D,327S/D_rev was used for mutating the 321 and 327 sites into aspartic acids. Plasmid pXL108 was used as template. After sequencing, the resulting plasmids pXL123(AAA) and pXL124(DDD), which harbor the triple mutation, were generated. Then the plasmids were transformed into the Δ*apsB* deletion strain, resulting in strains SXL180 and SXL181, respectively (Table S2).

Mass spectrometry after pulldown with PlkA and ApsB

Strains SXL137 (PlkA-GFP), SYZ2 (GFP-ApsB), SXL135 (Δ*plkA*; GFP-ApsB) as well as control strains only expressing GFP were incubated in 500 ml MM liquid medium (2% glycerol and 0.2% glucose) with appropriate auxotrophic markers at 37°C for 24 h. After that, the hyphae were collected, washed and performed with GFP-trap according to procedures form Chromotek (gta-20 agarose beads). PlkA and ApsB were pulled down with anti-GFP conjugated beads followed by elution with 2 × SD loading dye and detected with anti-GFP N-terminal mouse monoclonal antibody (Sigmal-Aldrich) in western blots. The immunoprecipitated proteins were loaded onto an SDS-PAGE gel and just run into the separating gel. Then the polyacrylamide gels were cut into pieces and subsequently subjected to tryptic in-gel digestion (Shevchenko et al., 1996). The used trypsin was sequencing grade modified from Promega. Dried peptide pellets were stored at 4°C until liquid chromatography-mass spectrometry (LC-MS) analysis.

Peptides were purified using C18 Stop and go extraction (Stage) tips (Rappsilber et al., 2003, 2007). Dried peptides were dissolved in 20 µl sample buffer (2% acetonitrile, 0.1% formic acid) whereof 2 µl were subjected to LC-MS analysis. Peptides were separated on Acclaim PepMap RSLC columns (Thermo Fisher Scientific) at nano-flow rates (300 nl/min) by running water-acetonitrile gradients on an Ultimate 3000 LC system online coupled to either an Orbitrap Velos Pro mass spectrometer or an Q Exactive HF mass spectrometer (instruments from Thermo Fisher Scientific). Peptides were on-line ionized by nano-electrospray ionization (nESI) using the Nanospray Flex Ion Source (Thermo Fisher Scientific) at 2.4 kV (Orbitrap Velos Pro) or 1.5 kV (Q Exactive HF) and continuously transferred into the respective mass spectrometer. Orbitrap Velos Pro: Full scans within the range of 300–1850 *m*/*z* were recorded with the Orbitrap-FT analyzer at a resolution of 30,000. In parallel, data-dependent top-ten fragmentation spectra (MS2) were acquired by collision-induced dissociation (CID) in the linear Velos ion trap. For Q Exactive HF, full scans were taken in a mass range of 300–1650 *m*/z and recorded at a resolution of 30,000 followed by data-dependent top 10 HCD fragmentation at a resolution of 15,000. The XCalibur software versions 2.2 and 4.0 (Thermo Fisher Scientific) were used for LC-MS method programming and data acquisition. MS/MS2 raw data processing for protein identification and analysis was carried out with the Proteome Discoverer 2.4 software (Thermo Fisher Scientific) using the SequestHT and Mascot search engines. An *A. nidulans*-specific protein database was used for the database search considering a maximum of two missed cleavage sites. Oxidation at methionine, N-terminal protein acetylation and phosphorylation of serine, threonine, and tyrosine were considered as variable modifications. Carbamidomethylation at cysteine was set as fixed modification. Phospho-site localization was evaluated using phosphoRS (Olsen et al., 2006; Olsen and Mann, 2004).

Light and fluorescence microscopy

For live-cell imaging, fresh spores were inoculated in 0.5 ml MM (2% glycerol for *alcA* promoter induction) with appropriate selection markers on

18×18 mm cover slip (Roth, Karlsruhe). The samples were incubated at 28°C overnight, followed by 2 h incubation at room temperature before microscopy. VECTASHIELD Mounting Medium with DAPI (Vector Laboratories) was used for staining nuclei in cells. Light and fluorescence images were taken with the Zeiss Microscope "AxioImager Z1" (Carl Zeiss, Jena, Germany) and the software ZEN pro 2012, using the Planapochromatic 63× oil immersion objective lens, and the Zeiss AxioCam MR camera. Image and video processing were undertaken with ZEN pro 2012, Adobe Photoshop or ImageJ (National Institutes of Health, MD, USA).

Alternatively, for *in vivo* time-lapse microscopy, cells were incubated in u-slide 8 well glass bottom dishes from Ibidi (cells in focus) in 0.5 ml MM plus 2% glycerol and appropriate supplements, and an additional 2 ml of medium added after overnight incubation. Movies were taken at a time-lapse interval of 5 s (for activity analysis) or 1 min (for mitosis progression), and maximum projections of a deconvolved *Z*-stack image were applied. For quantification of fluorescence intensity, images of 15–20 sections were taken along the *Z*-axis at 0.25-µm increments. After deconvolution, projection images of maximum intensity were obtained, and maximum fluorescence intensities over the background intensity were used for statistical data analysis. A 5×5-pixel region of interest (ROI) was selected and two 20×20-pixel regions around the ROI were used for background subtraction.

Calcofluor White staining was performed with M2R (fluorescent brightener 28 [F3543]; Sigma-Aldrich, Munich, Germany) at a 1:1000 dilution for 5 min immediately before microscopy).

High-resolution microscopy

For confocal imaging, samples were observed using an Axio Observer Z.1/LSM900 confocal microscope (Carl ZEISS microscopy) equipped with an oil-immersion objective (Plan Apochromat 63×/1.4; Carl ZEISS). Excitation laser wavelengths were 488 for EGFP and 561 nm for mCherry. Fluorescence signals were detected using the Airy scan detector with super resolution (SR) mode (https://www.embl.de/services/core_facilities/almf/events_ext/2017/EN_wp_LSM-880_Basic-Principle-Airyscan.pdf). Images were collected using the ZEN blue software (ZEISS). MT dynamics at hyphal tips were imaged for at least 1 min using the Airy scan detector in Multiplex 4Y mode.

Image analysis

Prior to time analysis, time-lapse movies of mitotic progression were bleach corrected using the bleach correction plugin (Correction Method: Simple Ratio) of ImageJ/Fiji. To analyze MT dynamics, time-lapse movies were converted into kymographs using the ZEN blue software (Zeiss). Quantification of MT dynamics was performed in ImageJ/Fiji using the Velocity measurement tool macro (http://dev.mri.cnrs.fr/projects/imagej-macros/wiki/Velocity_Measurement_Tool#Velocity-Measurement-Tool).

Statistical analysis

Significant differences were calculated using the two-tailed Mann–Whitney U test with GraphPad 8. *P*-values are denoted as $*P<0.05$; $**P<0.01$; $****P<0.0001$; ns, not significant.

Acknowledgements

We thank K. Schmitt for support in Mass spectrometry data analysis. We thank Gert Sonntag (Zeiss) for the opportunity and the help to use the LSM900 microscope. V.W. holds a fellowship from the German Federal Environmental Foundation (DBU).

Competing interests

The authors declare no competing or financial interests.

Author contributions

Conceptualization: R.F., X.G.; Methodology: X.G.; Validation: O.V.; Investigation: X.G., S.H., V.W., O.V.; Resources: S.E.; Data curation: X.G.; Writing - original draft: X.G.; Writing - review & editing: R.F.; Supervision: G.H.B., R.F.; Project administration: R.F.; Funding acquisition: R.F.

Funding

This work was supported by the German Science Foundation (Deutsche Forschungsgemeinschaft; DFG Fi459/20-1).

References

Archambault, V. and Glover, D. M. (2009). Polo-like kinases: conservation and divergence in their functions and regulation. *Nat. Rev. Mol. Cell Biol.* **10**, 265-275. doi:10.1038/nrm2653

Arquint, C., Gabryjonczyk, A.-M., Imseng, S., Böhm, R., Sauer, E., Hiller, S., Nigg, E. A. and Maier, T. (2015). STIL binding to Polo-box 3 of PLK4 regulates centriole duplication. *eLife* **4**, e07888. doi:10.7554/eLife.07888

Avena, J. S., Burns, S., Yu, Z., Ebmeier, C. C., Old, W. M., Jaspersen, S. L. and Winey, M. (2014). Licensing of yeast centrosome duplication requires phosphoregulation of sfi1. *PLoS Genet.* **10**, e1004666. doi:10.1371/journal.pgen.1004666

Bachewich, C., Masker, K. and Osmani, S. (2005). The polo-like kinase PLKA is required for initiation and progression through mitosis in the filamentous fungus *Aspergillus nidulans*. *Mol. Microbiol.* **55**, 572-587. doi:10.1111/j.1365-2958.2004.04404.x

Berlanga, J. J., Herrero, S. and de Haro, C. (1998). Characterization of the hemin-sensitive eukaryotic initiation factor 2α kinase from mouse nonerythroid cells. *J. Biol. Chem.* **273**, 32340-32346. doi:10.1074/jbc.273.48.32340

Bornens, M. (2012). The centrosome in cells and organisms. *Science* **335**, 422-426. doi:10.1126/science.1209037

Chen, P., Gao, R., Chen, S., Pu, L., Li, P., Huang, Y. and Lu, L. (2012). A pericentrin-related protein homolog in *Aspergillus nidulans* plays important roles in nucleus positioning and cell polarity by affecting microtubule organization. *Eukaryot. Cell* **11**, 1520-1530. doi:10.1128/EC.00203-12

Cheng, K.-Y., Lowe, E. D., Sinclair, J., Nigg, E. A. and Johnson, L. N. (2003). The crystal structure of the human polo–like kinase–1 polo box domain and its phospho–peptide complex. *EMBO J.* **22**, 5757-5768. doi:10.1093/emboj/cdg558

Coelho, P. A., Bury, L., Sharif, B., Riparbelli, M. G., Fu, J., Callaini, G., Glover, D. M. and Zernicka-Goetz, M. (2013). Spindle formation in the mouse embryo requires Plk4 in the absence of centrioles. *Dev. Cell* **27**, 586-597. doi:10.1016/j.devcel.2013.09.029

Conduit, P. T., Feng, Z., Richens, J. H., Baumbach, J., Wainman, A., Bakshi, S. D., Dobbelaere, J., Johnson, S., Lea, S. M. and Raff, J. W. (2014). The centrosome-specific phosphorylation of Cnn by Polo/Plk1 drives Cnn scaffold assembly and centrosome maturation. *Dev. Cell* **28**, 659-669. doi:10.1016/j.devcel.2014.02.013

Cota, R. R., Teixidó-Travesa, N., Ezquerra, A., Eibes, S., Lacasa, C., Roig, J. and Lüders, J. (2017). MZT1 regulates microtubule nucleation by linking γTuRC assembly to adapter-mediated targeting and activation. *J. Cell Sci.* **130**, 406-419. doi:10.1242/jcs.195321

de Cárcer, G., Manning, G. and Malumbres, M. (2011). From Plk1 to Plk5: functional evolution of polo-like kinases. *Cell Cycle* **10**, 2255-2262. doi:10.4161/cc.10.14.16494

De Souza, C. P., Hashmi, S. B., Hage, N., Fitch, R. M., Osmani, A. H. and Osmani, S. A. (2017). Location and functional analysis of the *Aspergillus nidulans* Aurora kinase confirm mitotic functions and suggest non-mitotic roles. *Fungal Genet. Biol.* **103**, 1-15. doi:10.1016/j.fgb.2017.03.004

Elia, A. E. H., Rellos, P., Haire, L. F., Chao, J. W., Ivins, F. J., Hoepker, K., Mohammad, D., Cantley, L. C., Smerdon, S. J. and Yaffe, M. B. (2003). The molecular basis for phosphodependent substrate targeting and regulation of Plks by the Polo-box domain. *Cell* **115**, 83-95. doi:10.1016/S0092-8674(03)00725-6

Elserafy, M., Šarić, M., Neuner, A., Lin, T.-c., Zhang, W., Seybold, C., Sivashanmugam, L. and Schiebel, E. (2014). Molecular mechanisms that restrict yeast centrosome duplication to one event per cell cycle. *Curr. Biol.* **24**, 1456-1466. doi:10.1016/j.cub.2014.05.032

Evers, D. M., Matta, J. A., Hoe, H.-S., Zarkowsky, D., Lee, S. H., Isaac, J. T. and Pak, D. T. S. (2010). Plk2 attachment to NSF induces homeostatic removal of GluA2 during chronic overexcitation. *Nat. Neurosci.* **13**, 1199-1207. doi:10.1038/nn.2624

Flory, M. R., Morphew, M., Joseph, J. D., Means, A. R. and Davis, T. N. (2002). Pcp1p, an Spc110p-related calmodulin target at the centrosome of the fission yeast *Schizosaccharomyces pombe*. *Cell Growth Differ.* **13**, 47-58.

Fong, C. S., Sato, M. and Toda, T. (2010). Fission yeast Pcp1 links polo kinase–mediated mitotic entry to γ–tubulin–dependent spindle formation. *EMBO J.* **29**, 120-130. doi:10.1038/emboj.2009.331

Gao, X., Schmid, M., Zhang, Y., Fukuda, S., Takeshita, N. and Fischer, R. (2019). The spindle pole body of *Aspergillus nidulans* is asymmetrical and contains changing numbers of γ-tubulin complexes. *J. Cell Sci.* **132**, jcs234799. doi:10.1242/jcs.234799

García-Álvarez, B., de Cárcer, G., Ibañez, S., Bragado-Nilsson, E. and Montoya, G. (2007). Molecular and structural basis of polo-like kinase 1 substrate recognition: Implications in centrosomal localization. *Proc. Natl. Acad. Sci. USA* **104**, 3107-3112. doi:10.1073/pnas.0609131104

Glover, D. M. (2005). Polo kinase and progression through M phase in *Drosophila*: a perspective from the spindle poles. *Oncogene* **24**, 230-237. doi:10.1038/sj.onc.1208279

Gönczy, P. (2015). Centrosomes and cancer: revisiting a long-standing relationship. *Nat. Rev. Cancer* **15**, 639-652. doi:10.1038/nrc3995

Habedanck, R., Stierhof, Y.-D., Wilkinson, C. J. and Nigg, E. A. (2005). The Polo kinase Plk4 functions in centriole duplication. *Nat. Cell Biol.* **7**, 1140-1146. doi:10.1038/ncb1320
Hill, T. W. and Käfer, E. (2001). Improved protocols for *Aspergillus* minimal medium: trace element and minimal medium salt stock solutions. *Fungal Genet. Rep.* **48**, 8. doi:10.4148/1941-4765.1173
Hu, F., Wang, Y., Liu, D., Li, Y., Qin, J. and Elledge, S. J. (2001). Regulation of the Bub2/Bfa1 GAP complex by Cdc5 and cell cycle checkpoints. *Cell* **107**, 655-665. doi:10.1016/S0092-8674(01)00580-3
Ito, D. and Bettencourt-Dias, M. (2018). Centrosome remodelling in evolution. *Cells* **7**, 71. doi:10.3390/cells7070071
James, S. W., Mirabito, P. M., Scacheri, P. C. and Morris, N. R. (1995). The *Aspergillus nidulans* bimE (blocked-in-mitosis) gene encodes multiple cell cycle functions involved in mitotic checkpoint control and mitosis. *J. Cell Sci.* **108**, 3485-3499. doi:10.1242/jcs.108.11.3485
Jang, Y.-J., Lin, C.-Y., Ma, S. and Erikson, R. L. (2002). Functional studies on the role of the C-terminal domain of mammalian polo-like kinase. *Proc. Natl. Acad. Sci. USA* **99**, 1984-1989. doi:10.1073/pnas.042689299
Jaspersen, S. L. and Winey, M. (2004). The budding yeast spindle pole body: structure, duplication, and function. *Annu. Rev. Cell Dev. Biol.* **20**, 1-28. doi:10.1146/annurev.cellbio.20.022003.114106
Keck, J. M., Jones, M. H., Wong, C. C. L., Binkley, J., Chen, D., Jaspersen, S. L., Holinger, E. P., Xu, T., Niepel, M., Rout, M. P. et al. (2011). A cell cycle phosphoproteome of the yeast centrosome. *Science* **332**, 1557-1561. doi:10.1126/science.1205193
Knop, M. and Schiebel, E. (1997). Spc98p and Spc97p of the yeast γ–tubulin complex mediate binding to the spindle pole body via their interaction with Spc110p. *EMBO J.* **16**, 6985-6995. doi:10.1093/emboj/16.23.6985
Knop, M. and Schiebel, E. (1998). Receptors determine the cellular localization of a γ–tubulin complex and thereby the site of microtubule formation. *EMBO J.* **17**, 3952-3967. doi:10.1093/emboj/17.14.3952
Kollman, J. M., Polka, J. K., Zelter, A., Davis, T. N. and Agard, D. A. (2010). Microtubule nucleating γ-TuSC assembles structures with 13-fold microtubule-like symmetry. *Nature* **466**, 879-882. doi:10.1038/nature09207
Konzack, S., Rischitor, P. E., Enke, C. and Fischer, R. (2005). The role of the kinesin motor KipA in microtubule organization and polarized growth of *Aspergillus nidulans*. *Mol. Biol. Cell* **16**, 433-1011. doi:10.1091/mbc.e04-02-0083
Lee, K. and Rhee, K. (2011). PLK1 phosphorylation of pericentrin initiates centrosome maturation at the onset of mitosis. *J. Cell Biol.* **195**, 1093-1101. doi:10.1083/jcb.201106093
Lee, K. S., Grenfell, T. Z., Yarm, F. R. and Erikson, R. L. (1998). Mutation of the polo-box disrupts localization and mitotic functions of the mammalian polo kinase Plk. *Proc. Natl. Acad. Sci. USA* **95**, 9301-9306. doi:10.1073/pnas.95.16.9301
Lee, K. S., Park, J.-E., Asano, S. and Park, C. J. (2005). Yeast polo-like kinases: functionally conserved multitask mitotic regulators. *Oncogene* **24**, 217-229. doi:10.1038/sj.onc.1208271
Lettman, M. M., Wong, Y. L., Viscardi, V., Niessen, S., Chen, S.-h., Shiau, A. K., Zhou, H., Desai, A. and Oegema, K. (2013). Direct binding of SAS-6 to ZYG-1 recruits SAS-6 to the mother centriole for cartwheel assembly. *Dev. Cell* **25**, 284-298. doi:10.1016/j.devcel.2013.03.011
Lin, T.-C., Neuner, A., Schlosser, Y. T., Scharf, A. N., Weber, L. and Schiebel, E. (2014). Cell-cycle dependent phosphorylation of yeast pericentrin regulates γ-TuSC-mediated microtubule nucleation. *eLife* **3**, e02208. doi:10.7554/eLife.02208
Lin, T.-C., Neuner, A. and Schiebel, E. (2015). Targeting of γ-tubulin complexes to microtubule organizing centers: conservation and divergence. *Trends Cell Biol.* **25**, 296-307. doi:10.1016/j.tcb.2014.12.002
Liu, J. and Maller, J. L. (2005). Xenopus Polo-like kinase Plx1: a multifunctional mitotic kinase. *Oncogene* **24**, 238-247. doi:10.1038/sj.onc.1208220
Liu, P., Zupa, E., Neuner, A., Böhler, A., Loerke, J., Flemming, D., Ruppert, T., Rudack, T., Peter, C., Spahn, C. et al. (2020). Insights into the assembly and activation of the microtubule nucleator γ-TuRC. *Nature* **578**, 467-471. doi:10.1038/s41586-019-1896-6
Martin, M. A., Osmani, S. A. and Oakley, B. R. (1997). The role of gamma-tubulin in mitotic spindle formation and cell cycle progression in *Aspergillus nidulans*. *J. Cell Sci.* **110**, 623-633. doi:10.1242/jcs.110.5.623
Masuda, H. and Toda, T. (2016). Synergistic role of fission yeast Alp16^{GCP6} and Mzt1^{MOZART1} in γ-tubulin complex recruitment to mitotic spindle pole bodies and spindle assembly. *Mol. Biol. Cell* **27**, 1753-1763. doi:10.1091/mbc.e15-08-0577
Mogilevsky, K., Glory, A. and Bachewich, C. (2012). The Polo-like kinase PLKA in *Aspergillus nidulans* is not essential but plays important roles during vegetative growth and development. *Eukaryot. Cell* **11**, 194-205. doi:10.1128/EC.05130-11
Morris, N. R. (1975). Mitotic mutants of *Aspergillus nidulans*. *Genet. Res.* **26**, 237-254. doi:10.1017/S0016672300016049
Moyer, T. C., Clutario, K. M., Lambrus, B. G., Daggubati, V. and Holland, A. J. (2015). Binding of STIL to Plk4 activates kinase activity to promote centriole assembly. *J. Cell Biol.* **209**, 863-878. doi:10.1083/jcb.201502088
Mulvihill, D. P. and Hyams, J. S. (2002). Cytokinetic actomyosin ring formation and septation in fission yeast are dependent on the full recruitment of the polo-like kinase Plo1 to the spindle pole body and a functional spindle assembly checkpoint. *J. Cell Sci.* **115**, 3575-3586. doi:10.1242/jcs.00031
Nguyen, T., Vinh, D. B. N., Crawford, D. K. and Davis, T. N. (1998). A genetic analysis of interactions with Spc110p reveals distinct functions of Spc97p and Spc98p, components of the yeast γ-tubulin complex. *Mol. Biol. Cell* **9**, 1951-2335. doi:10.1091/mbc.9.8.2201
Nigg, E. A. and Raff, J. W. (2009). Centrioles, centrosomes, and cilia in health and disease. *Cell* **139**, 663-678. doi:10.1016/j.cell.2009.10.036
Oakley, C. E. and Oakley, B. R. (1989). Identification of γ-tubulin, a new member of the tubulin superfamily encoded by mipA gene of *Aspergillus nidulans*. *Nature* **338**, 662-664. doi:10.1038/338662a0
Oakley, B. R., Oakley, C. E., Yoon, Y. and Jung, M. K. (1990). γ-Tubulin is a component of the spindle pole body that is essential for microtubule function in *Aspergillus nidulans*. *Cell* **61**, 1289-1301. doi:10.1016/0092-8674(90)90693-9
Olsen, J. V. and Mann, M. (2004). Improved peptide identification in proteomics by two consecutive stages of mass spectrometric fragmentation. *Proc. Natl. Acad. Sci. USA* **101**, 13417-13422. doi:10.1073/pnas.0405549101
Olsen, J. V., Blagoev, B., Gnad, F., Macek, B., Kumar, C., Mortensen, P. and Mann, M. (2006). Global, in vivo, and site-specific phosphorylation dynamics in signaling networks. *Cell* **127**, 635-648. doi:10.1016/j.cell.2006.09.026
Osmani, S. A., May, G. S. and Morris, N. R. (1987). Regulation of the mRNA levels of nimA, a gene required for the G2-M transition in *Aspergillus nidulans*. *J. Cell Biol.* **104**, 1495-1504. doi:10.1083/jcb.104.6.1495
Osmani, A. H., McGuire, S. L. and Osmani, S. A. (1991). Parallel activation of the NIMA and p34cdc2 cell cycle-regulated protein kinases is required to initiate mitosis in *A. nidulans*. *Cell* **67**, 283-291. doi:10.1016/0092-8674(91)90180-7
Pereira, G., Knop, M. and Schiebel, E. (1998). Spc98p directs the yeast γ-tubulin complex into the nucleus and is subject to cell cycle-dependent phosphorylation on the nuclear side of the spindle pole body. *Mol. Biol. Cell* **9**, 775-793. doi:10.1091/mbc.9.4.775
Petronczki, M., Lénárt, P. and Peters, J.-M. (2008). Polo on the rise—from mitotic entry to cytokinesis with Plk1. *Dev. Cell* **14**, 646-659. doi:10.1016/j.devcel.2008.04.014
Prigozhina, N. L., Oakley, C. E., Lewis, A. M., Nayak, T., Osmani, S. A. and Oakley, B. R. (2004). γ-Tubulin plays an essential role in the coordination of mitotic events. *Mol. Biol. Cell* **15**, 1486. doi:10.1091/mbc.e03-06-0405
Pu, R. T. and Osmani, S. A. (1995). Mitotic destruction of the cell cycle regulated NIMA protein kinase of *Aspergillus nidulans* is required for mitotic exit. *EMBO J.* **14**, 995-1003. doi:10.1002/j.1460-2075.1995.tb07080.x
Rahal, R. and Amon, A. (2008). The Polo-like kinase Cdc5 interacts with FEAR network components and Cdc14. *Cell Cycle* **7**, 3262-3272. doi:10.4161/cc.7.20.6852
Ramani, A., Mariappan, A., Gottardo, M., Mandad, S., Urlaub, H., Avidor-Reiss, T., Riparbelli, M., Callaini, G., Debec, A. and Feederle, R. (2018). Plk1/Polo phosphorylates Sas-4 at the onset of mitosis for an efficient recruitment of pericentriolar material to centrosomes. *Cell Rep.* **25**, 3618-3630.e6. doi:10.1016/j.celrep.2018.11.102
Rappsilber, J., Ishihama, Y. and Mann, M. (2003). Stop and go extraction tips for matrix-assisted laser desorption/ionization, nanoelectrospray, and LC/MS sample pretreatment in proteomics. *Anal. Chem.* **75**, 663-670. doi:10.1021/ac026117i
Rappsilber, J., Mann, M. and Ishihama, Y. (2007). Protocol for micro-purification, enrichment, pre-fractionation and storage of peptides for proteomics using StageTips. *Nat. Protoc.* **2**, 1896-1906. doi:10.1038/nprot.2007.261
Sakchaisri, K., Asano, S., Yu, L.-R., Shulewitz, M. J., Park, C. J., Park, J.-E., Cho, Y.-W., Veenstra, T. D., Thorner, J. and Lee, K. S. (2004). Coupling morphogenesis to mitotic entry. *Proc. Natl. Acad. Sci. USA* **101**, 4124-4129. doi:10.1073/pnas.0400641101
Sambrook, J. and Russel, D. W. (1999). *Molecular Cloning: A Laboratory Manual*. Cold Spring Harbor, New York: Cold Spring Harbor Laboratory Press.
Samejima, I., Miller, V. J., Rincon, S. A. and Sawin, K. E. (2010). Fission yeast Mto1 regulates diversity of cytoplasmic microtubule organizing centers. *Curr. Biol.* **20**, 1959-1965. doi:10.1016/j.cub.2010.10.006
Sawin, K. E., Lourenco, P. C. C. and Snaith, H. A. (2004). Microtubule nucleation at non-spindle pole body microtubule-organizing centers requires fission yeast centrosomin-related protein mod20p. *Curr. Biol.* **14**, 763-775. doi:10.1016/j.cub.2004.03.042
Shen, K.-F., Osmani, A. H., Govindaraghavan, M. and Osmani, S. A. (2014). Mitotic regulation of fungal cell-to-cell connectivity through septal pores involves the NIMA kinase. *Mol. Biol. Cell* **25**, 763-775. doi:10.1091/mbc.e13-12-0718
Shevchenko, A., Wilm, M., Vorm, O. and Mann, M. (1996). Mass spectrometric sequencing of proteins from silver-stained polyacrylamide gels. *Anal. Chem.* **68**, 850-858. doi:10.1021/ac950914h
Smits, V. A. J., Klompmaker, R., Arnaud, L., Rijksen, G., Nigg, E. A. and Medema, R. H. (2000). Polo-like kinase-1 is a target of the DNA damage checkpoint. *Nat. Cell Biol.* **2**, 672-676. doi:10.1038/35023629
Snead, J. L., Sullivan, M., Lowery, D. M., Cohen, M. S., Zhang, C., Randle, D. H., Taunton, J., Yaffe, M. B., Morgan, D. O. and Shokat, K. M. (2007). A coupled chemical-genetic and bioinformatic approach to Polo-like kinase pathway exploration. *Chem. Biol.* **14**, 1261-1272. doi:10.1016/j.chembiol.2007.09.011

Song, S. and Lee, K. S. (2001). A novel function of *Saccharomyces cerevisiae* CDC5 in cytokinesis. *J. Cell Biol.* **152**, 451-470. doi:10.1083/jcb.152.3.451
Song, S., Grenfell, T. Z., Garfield, S., Erikson, R. L. and Lee, K. S. (2000). Essential function of the polo box of Cdc5 in subcellular localization and induction of cytokinetic structures. *Mol. Cell. Biol.* **20**, 286-298. doi:10.1128/MCB.20.1.286-298.2000
Soues, S. and Adams, I. R. (1998). SPC72: a spindle pole component required for spindle orientation in the yeast *Saccharomyces cerevisiae*. *J. Cell Sci.* **111**, 2809-2818. doi:10.1242/jcs.111.18.2809
Suelmann, R., Sievers, N., Galetzka, D., Robertson, L., Timberlake, W. E. and Fischer, R. (1998). Increased nuclear traffic chaos in hyphae of *Aspergillus nidulans:* molecular characterization of *apsB* and *in vivo* observation of nuclear behaviour. *Mol. Microbiol.* **30**, 831-842. doi:10.1046/j.1365-2958.1998.01115.x
Szewczyk, E. and Oakley, B. R. (2011). Microtubule dynamics in mitosis in *Aspergillus nidulans*. *Fungal Genet. Biol.* **48**, 998-999. doi:10.1016/j.fgb.2011.07.003
Takaki, T., Trenz, K., Costanzo, V. and Petronczki, M. (2008). Polo-like kinase 1 reaches beyond mitosis—cytokinesis, DNA damage response, and development. *Curr. Opin. Cell Biol.* **20**, 650-660. doi:10.1016/j.ceb.2008.10.005
Tanaka, K., Petersen, J., MacIver, F., Mulvihill, D. P., Glover, D. M. and Hagan, I. M. (2001). The role of Plo1 kinase in mitotic commitment and septation in *Schizosaccharomyces pombe*. *EMBO J.* **20**, 1259-1270. doi:10.1093/emboj/20.6.1259
Teixidó-Travesa, N., Roig, J. and Lüders, J. (2012). The where, when and how of microtubule nucleation–one ring to rule them all. *J. Cell Sci.* **125**, 4445-4456. doi:10.1242/jcs.106971
Todd, R. B., Davis, M. A. and Hynes, M. J. (2007). Genetic manipulation of *Aspergillus nidulans*: meiotic progeny for genetic analysis and strain construction. *Nat. Protoc.* **2**, 811-821. doi:10.1038/nprot.2007.112
Vogel, J., Drapkin, B., Oomen, J., Beach, D., Bloom, K. and Snyder, M. (2001). Phosphorylation of γ-tubulin regulates microtubule organization in budding yeast. *Dev. Cell* **1**, 621-631. doi:10.1016/S1534-5807(01)00073-9
Wälde, S. and King, M. C. (2014). The KASH protein Kms2 coordinates mitotic remodeling of the spindle pole body. *J. Cell Sci.* **127**, 3625-3640. doi:10.1242/jcs.154997
Waring, R. B., May, G. S. and Morris, N. R. (1989). Characterization of an inducible expression system in *Aspergillus nidulans* using *alcA* and tubulincoding genes. *Gene* **79**, 119-130. doi:10.1016/0378-1119(89)90097-8
Wilson, E. B. (1925). *Cell In Development And Heredity*, 3rd edn. New York: Rev: Macmillan Company.
Xiong, Y. and Oakley, B. R. (2009). *In vivo* analysis of the functions of γ-tubulin-complex proteins. *J. Cell Sci.* **122**, 4218-4227. doi:10.1242/jcs.059196
Yang, L., Ukil, L., Osmani, A., Nahm, F., Davies, J., De Souza, C. P. C., Dou, X., Perez-Balaguer, A. and Osmani, S. A. (2004). Rapid production of gene replacement constructs and generation of a green fluorescent protein-tagged centromeric marker in *Aspergillus nidulans*. *Eukaryot. Cell* **3**, 1359-1362. doi:10.1128/EC.3.5.1359-1362.2004
Yelton, M. M., Hamer, J. E. and Timberlake, W. E. (1984). Transformation of *Aspergillus nidulans* by using a *trpC* plasmid. *Proc. Natl. Acad. Sci. USA* **81**, 1470-1474. doi:10.1073/pnas.81.5.1470
Zekert, N., Veith, D. and Fischer, R. (2010). Interaction of the *Aspergillus nidulans* microtubule-organizing center (MTOC) component ApsB with gamma-tubulin and evidence for a role of a subclass of peroxisomes in the formation of septal MTOCs. *Eukaryot. Cell* **9**, 795-805. doi:10.1128/EC.00058-10
Zhang, Y., Gao, X., Manck, R., Schmid, M., Osmani, A. H., Osmani, S. A., Takeshita, N. and Fischer, R. (2017). Microtubule-organizing centers of *Aspergillus nidulans* are anchored at septa by a disordered protein. *Mol. Microbiol.* **106**, 285-303. doi:10.1111/mmi.13763
Zheng, Y., Wong, M. L., Alberts, B. and Mitchison, T. (1995). Nucleation of microtubule assembly by a γ-tubulin-containing ring complex. *Nature* **378**, 578. doi:10.1038/378578a0
Zitouni, S., Nabais, C., Jana, S. C., Guerrero, A. and Bettencourt-Dias, M. (2014). Polo-like kinases: structural variations lead to multiple functions. *Nat. Rev. Mol. Cell Biol.* **15**, 433-452. doi:10.1038/nrm3819
Zitouni, S., Francia, M. E., Leal, F., Gouveia, S. M., Nabais, C., Duarte, P., Gilberto, S., Brito, D., Moyer, T., Kandels-Lewis, S. et al. (2016). CDK1 prevents unscheduled PLK4-STIL complex assembly in centriole biogenesis. *Curr. Biol.* **26**, 1127-1137. doi:10.1016/j.cub.2016.03.055

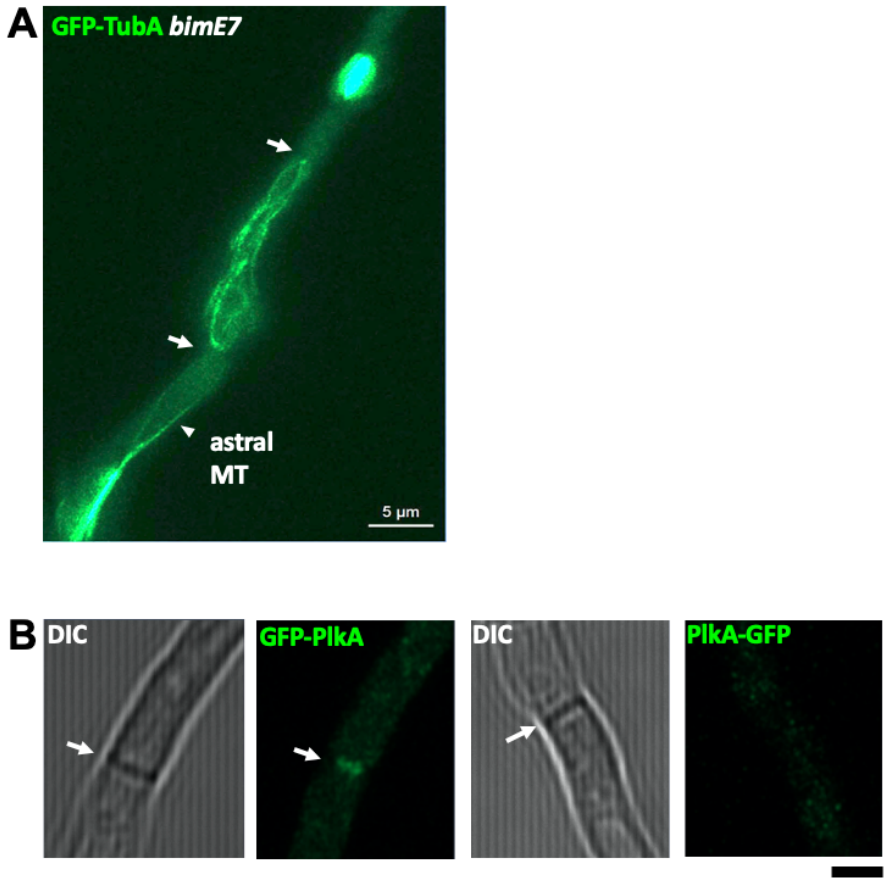

Fig. S1. (A) Study of sMTOC activities in interphase and in two compartments blocked in mitosis (left picture). Strains SXL136 (*alcA(p)::GFP::tubA*; *bimE7*) was incubated in MM (2% glycerol with auxotrophic markers) at 28°C overnight followed by 42°C treatment for 4h to block mitosis. Arrows indicate septa. Scale bar, 5µm. **(B)** GFP fusion at the C-terminus of PlkA abolished the septa localization. Strains SXL164 (*alcA(p)::GFP::plkA*) and SXL137 (*plkA::GFP*) were incubated in MM (2% glycerol) with supplements at 28°C overnight. Arrows indicate the septa positions. Scale bar, 2 µm.

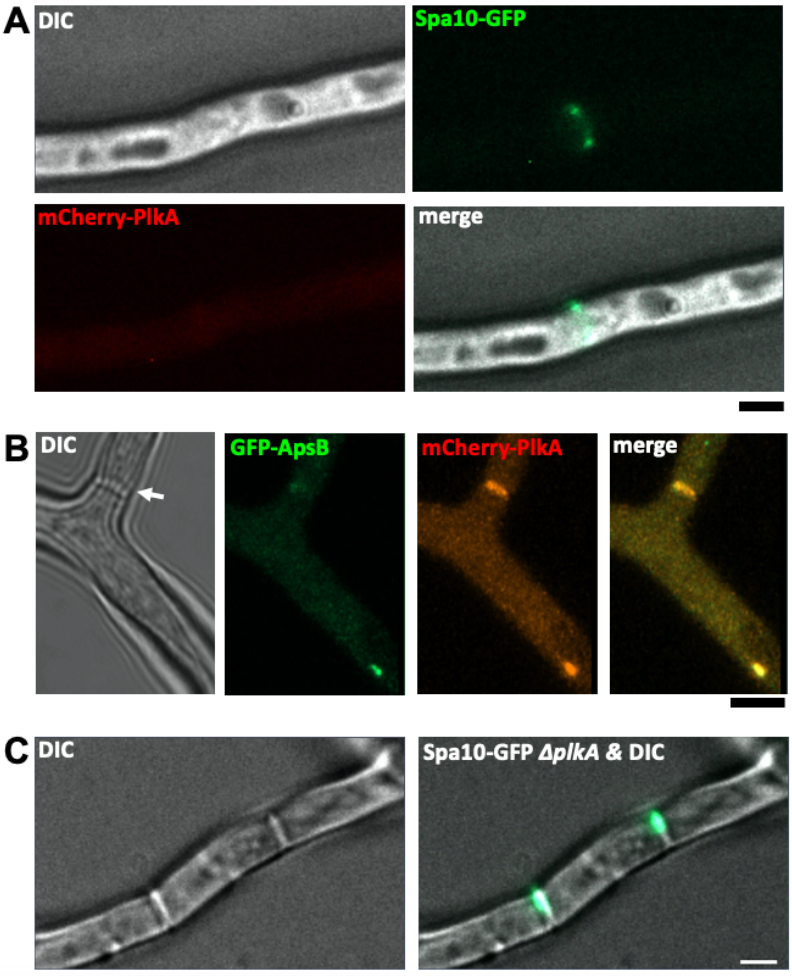

Fig. S2. (A) Analysis of PlkA and Spa10 localizations at septa. Spa10 localizes to forming septa earlier than PlkA. At the beginning of septation, where Spa10 localizes as a constriction ring, PlkA is not yet appeared. Strain SXL179 (*alcA(p)::mCherry::plkA; spa10::GFP*) was incubated in MM (2% glycerol) at 28°C overnight and observed. Scale bar, 2 µm. (**B**) PlkA localizes to forming septa earlier than ApsB. Arrows indicate the position of a forming septum. Strains SXL174 (*alcA(p)::mCherry::plkA*; *alcA(p)::GFP::apsB*) was incubated as above. Pictures were taken with the LSM 980 Airyscan microscope. Scale bar, 2µm. **(C)** Spa10 localization to mature septa was unaffected in the absence of PlkA. Strain SXL182 (Δ*plkA; spa10::GFP*) was incubated as above and observed. Scale bar, 2 µm.

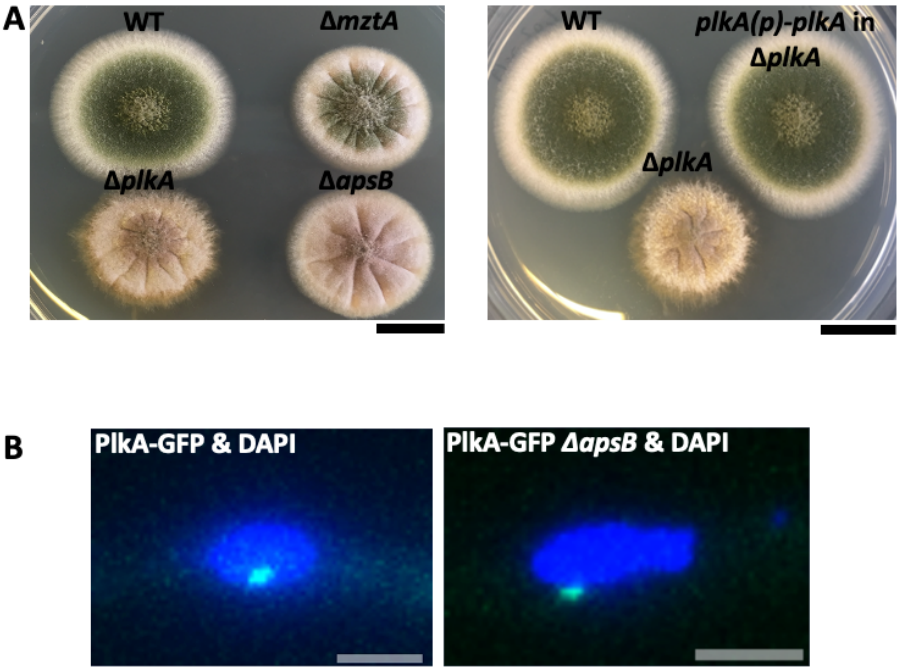

Fig. S3. (A) Phenotype of a *plkA-deletion* strain. Comparison of colonies in WT, Δ*mztA,* Δ*apsB,* and Δ*plkA* (left) and re-complementation of Δ*plkA* (right). Strains TN02A3 (WT), SXL49 (Δ*mztA*), SYZ3 (Δ*apsB*) and SXL122 (Δ*plkA*) were incubated in MM plate with supplements for three days. Scale bar 1cm. **(B)** Localization of PlkA was not affected in the absence of ApsB. Strains SXL137 (*plkA::GFP*) and SXL138 (*plkA::GFP;* Δ*apsB*) were incubated in MM (2% glycerol) with supplements at 28°C overnight. Nuclei were stained with DAPI.

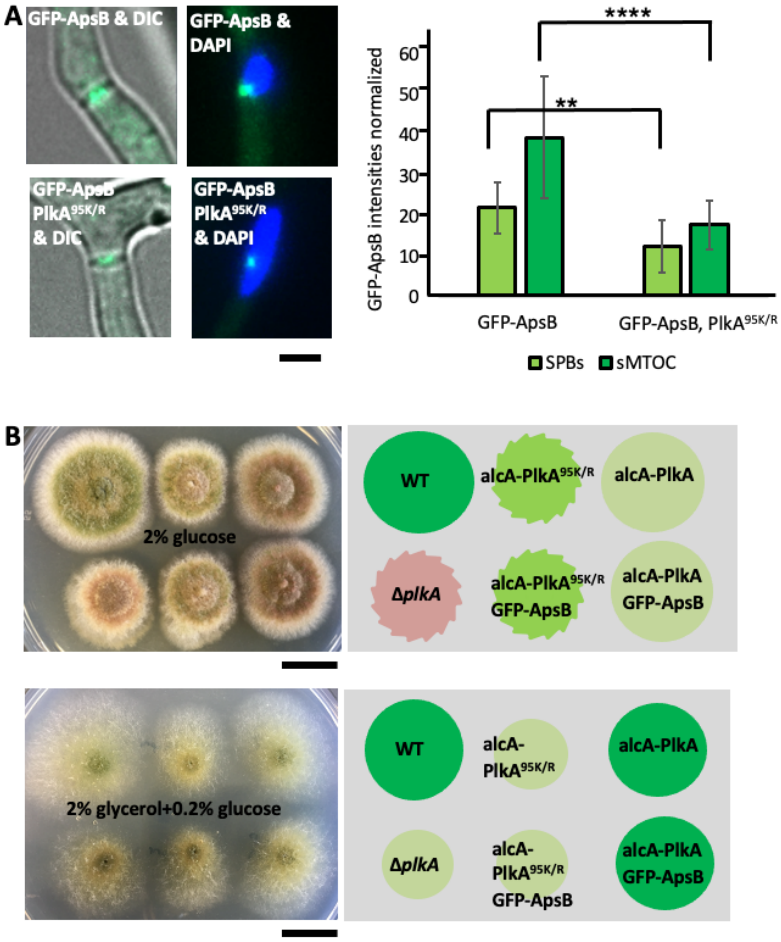

Fig. S4. Analyzing the catalytic role of PlkA. (A) Images of GFP-ApsB signal intensities at sMTOCs and SPBs in WT PlkA and mutated PlkA$^{95K/R}$. Strains SXL174 (*alcA(p)::GFP::apsB; alcA(p)::mCherry::plkA*) and SXL175 (*alcA(p)::GFP::apsB; alcA(p)::mCherry::plkA^{95R}*) were incubates in MM (2% glycerol) at 28°C overnight and imaged. Nuclei were stained with DAPI. Scale bar, 2 µm. Localization of ApsB at SPBs and sMTOCs are significantly reduced in catalytic mutant of *plkA.* Totally 30 SPBs and 15 sMTOCs were calculated for each strain. The vertical lines mark the region of the SD. Mann-Whitney U tests were performed with GraphPad Prism 8. The asterisks **** above the graph indicate significant differences compared to wild type ($p < 0.0001$). **(B)** Comparison of the phenotype in WT, Δ*plkA and plkA^{95R}* in repressing (upper) and de-repressing (lower) plates. Strains TN02A3 (WT), SXL122 (Δ*plkA*), SXL158 (*alcA(p)::mCherry::plkA*), SXL159 (*alcA(p)::mCherry::plkA^{95R}*), SXL174 (*alcA(p)::GFP::apsB; alcA(p)::mCherry::plkA*) and SXL175 (*alcA(p)::GFP::apsB; alcA(p)::mCherry::plkA^{95R}*) were incubated in MM plates (2% glucose for repressing *alcA* promoter and 2% glycerol for de-repressing) with supplements for three days. Scale bar 1cm.

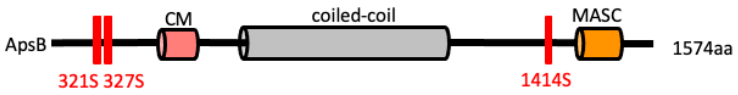

#1	b+	b2+	Seq.	y+	y2+	#2
1	114.09134	57.54931	L			15
2	261.15975	131.08352	F	1491.57476	746.29102	14
3	348.19178	174.59953	S	1344.50634	672.75681	13
4	463.21873	232.11300	D	1257.47431	629.24080	12
5	520.24019	260.62373	G	1142.44737	571.72732	11
6	634.28312	317.64520	N	1085.42591	543.21659	10
7	733.35153	367.17940	V	971.38298	486.19513	9
8	900.34989	450.67858	S-Phospho	872.31457	436.66092	8
9	1015.37683	508.19205	D	705.31621	353.16174	7
10	1086.41395	543.71061	A	590.28926	295.64827	6
11	1201.44089	601.22408	D	519.25215	260.12971	5
12	1272.47800	636.74264	A	404.22521	202.61624	4
13	1343.51512	672.26120	A	333.18809	167.09769	3
14	1430.54715	715.77721	S	262.15098	131.57913	2
15			R	175.11895	88.06311	1

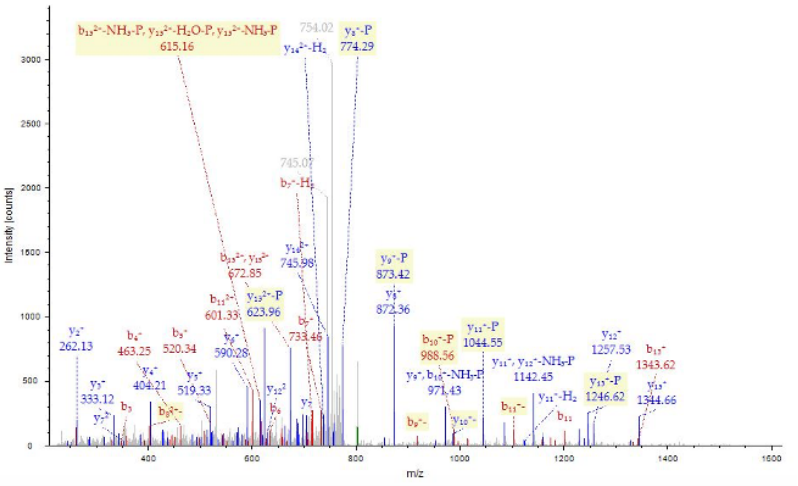

Fig. S5. Annotated fragmentation spectrum and ion series for the peptide LFSDGNVSDADAASR phosphorylated at S321 (34% isolation interference; Proteome Discoverer 2.2)**.**

#1	b+	b2+	Seq.	y+	y2+	#2
1	114.09134	57.54931	L			15
2	261.15975	131.08352	F	1491.57476	746.29102	14
3	348.19178	174.59953	S	1344.50634	672.75681	13
4	463.21873	232.11300	D	1257.47431	629.24080	12
5	520.24019	260.62373	G	1142.44737	571.72732	11
6	634.28312	317.64520	N	1085.42591	543.21659	10
7	733.35153	367.17940	V	971.38298	486.19513	9
8	820.38356	410.69542	S	872.31457	436.66092	8
9	935.41050	468.20889	D	785.28254	393.14491	7
10	1006.44762	503.72745	A	670.25560	335.63144	6
11	1121.47456	561.24092	D	599.21848	300.11288	5
12	1192.51167	596.75947	A	484.19154	242.59941	4
13	1263.54879	632.27803	A	413.15443	207.08085	3
14	1430.54715	715.77721	S-Phospho	342.11731	171.56229	2
15			R	175.11895	88.06311	1

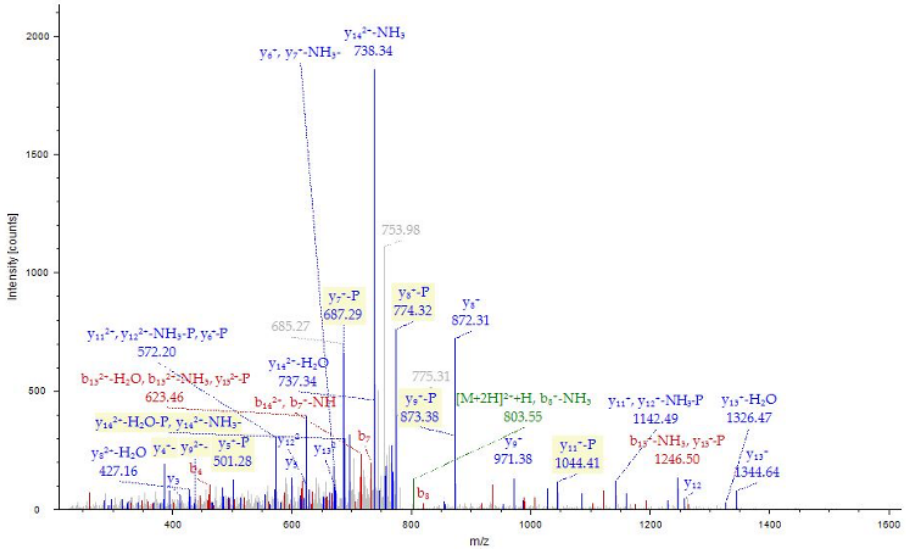

Fig. S6. Annotated fragmentation spectrum and ion series for the peptide LFSDGNVSDADAASR phosphorylated at S327 (15% isolation interference; Proteome Discoverer 2.2)**.**

#1	b⁺	b²⁺	Seq.	y⁺	y²⁺	#2
1	88.03930	44.52329	S			20
2	189.08698	95.04713	T	1940.89609	970.95168	19
3	290.13466	145.57097	T	1839.84841	920.42784	18
4	361.17178	181.08953	A	1738.80073	869.90401	17
5	418.19324	209.60026	G	1667.76362	834.38545	16
6	517.26165	259.13446	V	1610.74216	805.87472	15
7	588.29877	294.65302	A	1511.67374	756.34051	14
8	645.32023	323.16375	G	1440.63663	720.82195	13
9	812.31859	406.66293	S-Phospho	1383.61517	692.31122	12
10	909.37135	455.18932	P	1216.61681	608.81204	11
11	1037.42993	519.21860	Q	1119.56404	560.28566	10
12	1124.46196	562.73462	S	991.50546	496.25637	9
13	1211.49399	606.25063	S	904.47344	452.74036	8
14	1312.54167	656.77447	T	817.44141	409.22434	7
15	1425.62573	713.31650	I	716.39373	358.70050	6
16	1540.65267	770.82997	D	603.30967	302.15847	5
17	1653.73674	827.37201	L	488.28272	244.64500	4
18	1724.77385	862.89056	A	375.19866	188.10297	3
19	1853.81644	927.41186	E	304.16155	152.58441	2
20			R	175.11895	88.06311	1

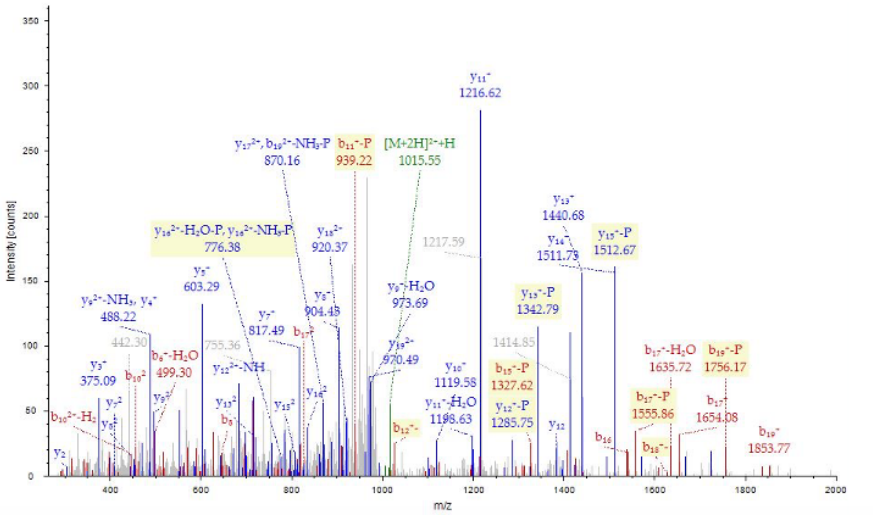

Fig. S7. Annotated fragmentation spectrum and ion series for the peptide STTAGVAGSPQSSTIDLAER phosphorylated at S1414 (7% isolation interference; Proteome Discoverer 2.2).

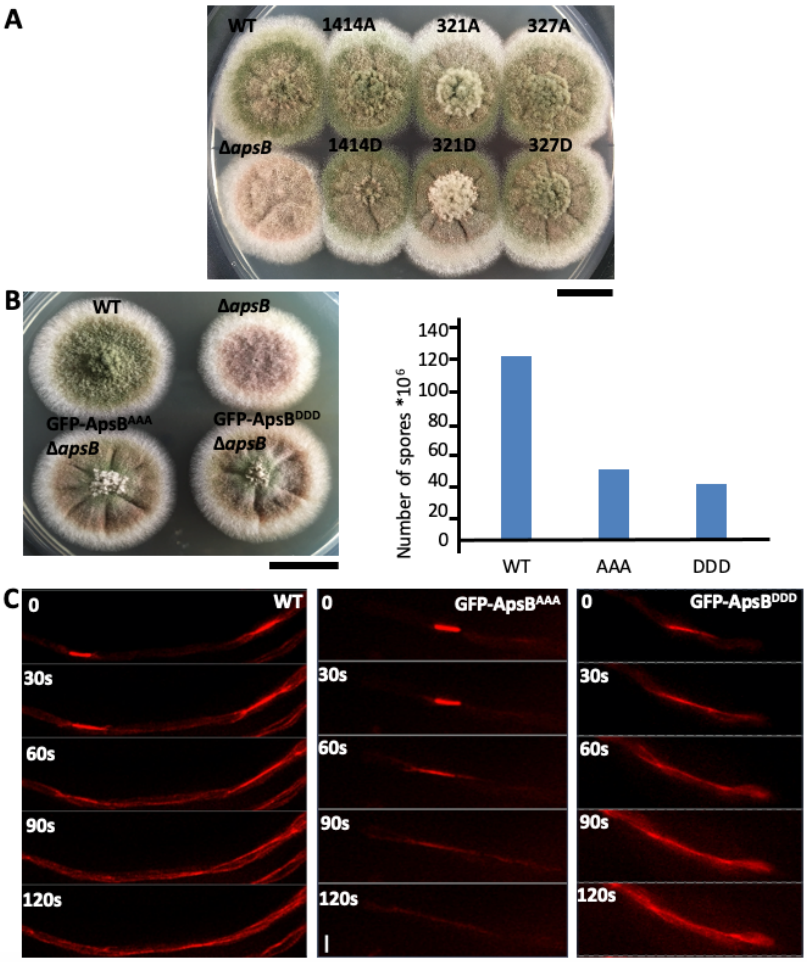

Fig. S8. (A) Single mutation of ApsB phosphorylation sites to alanine or to aspartic acid does not affect its function and localization. Strains SYZ2 (*alcA(p)::GFP::apsB*^{WT}), SYZ3 (Δ*apsB*), SXL160 (Δ*apsB*; *alcA(p)::GFP::apsB*^{1414A}), SXL161 (Δ*apsB*; *alcA(p)::GFP::apsB*^{1414D}), SXL162 (Δ*apsB*; *alcA(p)::GFP::apsB*^{321A}), SXL163 (Δ*apsB*; *alcA(p)::GFP::apsB*^{321D}), SXL168 (Δ*apsB*; *alcA(p)::GFP::apsB*^{327A}) and SXL169 (Δ*apsB*; *alcA(p)::GFP::apsB*^{327D}) were grown on MM plate with 2% glucose for three days at 37°C. Scale bar, 1 cm. **(B)** Triple mutation of ApsB phosphorylation sites to A or to D partially rescues the deletion phenotype. Colony phenotype of triple mutations shows sporulation defects. Strains TN02A3 (WT), SYZ3 (Δ*apsB*), SXL180 (Δ*apsB*; *alcA(p)::GFP::apsB*^{AAA};*mCherry::tubA*), SXL181 (Δ*apsB*;*alcA(p)::GFP::apsB*^{DDD}; *mCherry::tubA*) were grown on MM plate with 2% glucose for three days and washed for spore counting. Scale bar, 1 cm. The spore numbers in triple mutants are highly decreased ($47.5*10^6$, $37.5*10^6$) compared to wild type ($122.5 *10^6$). **(C)** Mitotic process of triple mutants behaves normally. The same strains as in **B** were grown in 8 well u-slides at 28°C overnight for long term observation. Time lapse images were taken every 30s at room temperature. Scale bar, 2 µm.

Table S1. Protein identification details for PlkA-GFP capture. The experiment was performed in duplicate using a strain expressing free GFP as negative control. The Table lists the number of peptides and number of peptide spectrum matches (PSMs, SequestHT and Mascot) for the bait protein PlkA and the four tubulin proteins. In brackets, the total number of proteins identified with high FDR confidence is provided.

	Sample							
Protein	PlkA-GFP replicate 1 (313proteins identified)		PlkA-GFP replicate 2 (229 proteins identified)		GFP control replicate 1 (61 proteins identified)		GFP control replicate 2 (37 proteins identified)	
	# peptides	# PSMs	# peptides	# PSMs	# peptides	# PSMs	# peptides	# PSMs
PlkA	29	116	21	56	0	0	0	0
tubA (α tubulin)	10	24	5	12	1	2	0	0
tubB (α tubulin)	12	32	6	11	2	4	0	0
benA (β tubulin)	10	29	7	19	3	9	0	0
tubC (β tubulin)	7	24	4	13	2	7	0	0

Journal of Cell Science • Supplementary information

Table S2. List of *A. nidulans* strains used in this study

Strain	Genotype	Source
TN02A3	*pyrG89; argB2; pyroA4, ΔnkuA::argB; veA1*	(Nayak et al., 2006)
SJW65	*wA3; pyrG89; argB2; pyroA4, ΔnkuA::argB; alcA(p)::GFP::tubA::pyr4*	J. Warmboldt, Marburg
SJW02	*wA3; pyrG89; pyroA4; ΔargB::trpCΔB; alcA(p)::GFP::tubA::pyr4*	J. Warmboldt, Marburg
SSH62	*pyrG89; argB2; pyroA4, ΔnkuA::argB; alcA(p)::mCherry::tubA::pyroA*	(Takeshita et al., 2013)
SSH27	*wA3, alcA(p)::GFP::kipA::pyr4; ΔargB::trpCΔB*	(Herrero et al., 2011)
SNZ-SH80	*fwA1; pyrG89; chaA1, sE15, wA3; argB2; ΔnkuA::argB, pyroA4; nirA14; gcpC(p)::gcpC::GFP::AfpyrG;*	(Zekert et al., 2010)
SYZ2	*pyrG89*; *argB2*; *pyroA4*, Δ*nkuA*::*argB*; *alcA(p)*::*GFP*::*apsB*::*pyr4*	(Zhang et al., 2017)
SYZ3	*pyrG89*; *argB2*; *pyroA4*, Δ*nkuA*::*argB*; Δ*apsB*::*pyroA*	(Zhang et al., 2017)
SXL49	*pyrG89*; *argB2*; *pyroA4*, Δ*nkuA*::*argB*; Δ*mztA*::*pyroA*	(Gao et al., 2019)
SMS4	*pyrG89*; *argB2*; *pyroA4*, Δ*nkuA*::*argB*; *mztA::GFP::AfpyrG*	(Gao et al., 2019)
Only GFP	*yA2*; *pabaA1*; *gpdA(p)::GFP*	B. Joehnk, Göttingen
SO4	*bimE7*; *wA2*; *pabaA1*	(Osmani et al., 1991)

SO1191	*An-nup2-GFP:: AfpyrG*; *bimE7*; *riboA2*; *nicB8*; *yA2*	SA. Osmani, USA
SRM212	*pyrG89*; *argB2*; *pyroA4*, Δ*nkuA*::*argB*; *spa10::GFP::AfpyrG*	(Zhang et al., 2017)
SXW1	*pyrG89; argB2; pyroA4,* Δ*nkuA::argB; alcA(p)::mCherry::tubA::pyroA; alcA(p)::GFP::kipA::pyr4* (SSH transformed with pSK82)	This work
SXW7	*pyrG89; argB2; pyroA4,* Δ*nkuA::argB; alcA(p)::YFP^{N}::pcpA::pyroA ; alcA(p)::YFP^{C}::plkA::pyr4* (TN02A3 transformed with pXL58 and pXW8,homologous integration)	This work
SXL122	*pyrG89*; *argB2*; *pyroA4*, Δ*nkuA*::*argB*; Δ*plkA::pyroA* (TN02A3 transformed with pXL79 homologous integration)	This work
SXL124	*pyrG89*; *argB2*; *pyroA4*, Δ*nkuA*::*argB*; *alcA(p)::YFP^{N}::apsB::pyroA ; alcA(p)::YFP^{C}::plkA::pyr4* (TN02A3 transformed with pYZ59 and pXW8, homologous integration)	This work
SXL125	*pyrG89*; *argB2*; *pyroA4*, Δ*nkuA*::*argB*; *alcA(p)::YFP^{N}::pcpA::pyroA ; alcA(p)::YFP^{C}::plkA::pyr4* (TN02A3 transformed with pXL58 and pXW8,homologous integration)	This work
SXL126	*pyrG89*; *argB2*; *pyroA4*, Δ*nkuA*::*argB*; Δ*plkA::pyroA; plkA(p)::plkA::AfpyrG* (SXL122 transformed with pXL81)	This work
SXL129	*pyrG89; argB2; pyroA4,* Δ*nkuA::argB;* Δ*plkA::pyroA mztA(p)::mztA::GFP::AfpyrG* (SXL122 transformed with pXL23, homologous integration)	This work
SXL131	*pyrG89; argB2; pyroA4,* Δ*nkuA::argB;* Δ*plkA::pyroA gcpC(p)::gcpC::GFP::AfpyrG* (SXL122 transformed with *gcpC(C-terminal)::GFP::AfpyrG::gcpC(RB)* cassette, homologous integration)	This work
SXL133	*An-nup2-GFP::AfpyrG*; *bimE7* (SO1191 cross with 65)	This work
SXL134	*An-nup2-GFP::AfpyrG*; *bimE7*; Δ*plkA::pyroA* (SO1191 cross with SXL122)	This work

SXL135	*pyrG89*; *argB2*; *pyroA4*, Δ*nkuA*::*argB*; Δ*plkA::pyroA alcA(p)::GFP::apsB::pyr4* (SYZ2 cross with SXL122)	This work
SXL136	*wA3*; *argB2*; *alcA(p)::GFP::tubA::pyr4*; *bimE7* (SO4 cross with SJW02)	This work
SXL137	*pyrG89*; *argB2*; *pyroA4*, Δ*nkuA*::*argB*; *plkA(p)::plkA::GFP::AfpyrG* (TN02A3 transformed with pXL82, homologous integration)	This work
SXL138	*pyrG89*; *argB2*; *pyroA4*, Δ*nkuA*::*argB*; Δ*apsB::pyroA*; *plkA(p)::plkA::GFP::AfpyrG* (SYZ3 transformed with pXL82, homologous integration)	This work
SXL156	*pyrG89*; *argB2*; *pyroA4*, Δ*nkuA*::*argB*; Δ*apsB::pyroA*, *alcA(p)::GFP::apsB^{full}::pyr4* (SYZ3 transformed with pXL106)	This work
SXL158	*pyrG89*; *argB2*; *pyroA4*, Δ*nkuA*::*argB*; *alcA(p)::mCherry::plkA::pyroA* (TN02A3 transformed with pXL83 homologous integration)	This work
SXL159	*pyrG89*; *argB2*; *pyroA4*, Δ*nkuA*::*argB*; *alcA(p)::mCherry::plkA$^{95\ K\ to\ R}$::pyroA* (TN02A3 transformed with pXL114 homologous integration)	This work
SXL160	*pyrG89*; *argB2*; *pyroA4*, Δ*nkuA*::*argB*; Δ*apsB::pyroA*, *alcA(p)::GFP::apsB$^{1414S\ to\ A}$::pyr4* (SYZ3 transformed with pXL107)	This work
SXL161	*pyrG89*; *argB2*; *pyroA4*, Δ*nkuA*::*argB*; Δ*apsB::pyroA*, *alcA(p)::GFP::apsB$^{1414S\ to\ D}$::pyr4* (SYZ3 transformed with pXL108)	This work
SXL162	*pyrG89*; *argB2*; *pyroA4*, Δ*nkuA*::*argB*; Δ*apsB::pyroA*, *alcA(p)::GFP::apsB$^{321S\ to\ A}$::pyr4* (SYZ3 transformed with pXL109)	This work
SXL163	*pyrG89*; *argB2*; *pyroA4*, Δ*nkuA*::*argB*; Δ*apsB::pyroA*, *alcA(p)::GFP::apsB$^{321S\ to\ D}$::pyr4* (SYZ3 transformed with pXL110)	This work
SXL164	*pyrG89*; *argB2*; *pyroA4*, Δ*nkuA*::*argB*;	This work

	alcA(p)::GFP::plkA::pyr4 (TN02A3 transformed with pXL84)	
SXL168	*pyrG89*; *argB2*; *pyroA4*, Δ*nkuA*::*argB*; Δ*apsB::pyroA*, *alcA(p)::GFP::apsB*$^{327S\ to\ A}$*::pyr4* (SYZ3 transformed with pXL117)	This work
SXL169	*pyrG89*; *argB2*; *pyroA4*, Δ*nkuA*::*argB*; Δ*apsB::pyroA*, *alcA(p)::GFP::apsB*$^{327S\ to\ D}$*::pyr4* (SYZ3 transformed with pXL118)	This work
SXL174	*pyrG89*; *argB2*; *pyroA4*, Δ*nkuA*::*argB*; *alcA(p)::mCherry::plkA::pyroA;* *alcA(p)::GFP::apsB::pyr4* (SYZ2 crossed with SXL158)	This work
SXL175	*pyrG89*; *argB2*; *pyroA4*, Δ*nkuA*::*argB*; *alcA(p)::mCherry::plkA*$^{95\ K\ to\ R}$*::pyroA;* *alcA(p)::GFP::apsB::pyr4* (SYZ2 crossed with SXL159)	This work
SXL176	*pyrG89*; *argB2*; *pyroA4*, Δ*nkuA*::*argB*; *alcA(p)::mCherry::plkA::pyroA;* *alcA(p)::GFP::tubA::pyr4* (65 transformed with pXL83, homologous integration)	This work
SXL177	*pyrG89*; *argB2*; *pyroA4*, Δ*nkuA*::*argB*; Δ*plkA::pyroA; alcA(p)::GFP::tubA::pyr4* (65 transformed with plkA deletion cassette, homologous integration)	This work
SXL178	*pyrG89*; *argB2*; *pyroA4*, Δ*nkuA*::*argB*; *alcA(p)::mCherry::plkA*^{95R}*::pyroA;* *alcA(p)::GFP::tubA::pyr4* (SXL159 transformed with pXL32, homologous integration)	This work
SXL179	*pyrG89*; *argB2*; *pyroA4*, Δ*nkuA*::*argB*; *alcA(p)::mCherry::plkA::pyroA;* *spa10(p)::spa10::GFP::AfpyrG* (SRM212 crossed with SXL158)	This work
SXL180	*pyrG89*; *argB2*; *pyroA4*, Δ*nkuA*::*argB*; Δ*apsB::pyroA*, *alcA(p)::GFP::apsB*$^{321S\ to\ A;\ 327\ S\ to\ A;1414S\ to\ A}$*::pyr4*; *alcA(p)::mCherry::tubA::pyroA* (SYZ3 co-transformed with pXL123 and pSH44	This work
SXL181	*pyrG89*; *argB2*; *pyroA4*, Δ*nkuA*::*argB*; Δ*apsB::pyroA*, *alcA(p)::GFP::apsB*$^{321S\ to\ D;\ 327\ S\ to\ D;1414S\ to\ D}$*::pyr4*; *alcA(p)::mCherry::tubA::pyroA* (SYZ3 co-transformed with pXL124 and pSH44	This work

SXL182	*pyrG89*; *argB2*; *pyroA4*, *ΔnkuA*::*argB*; *ΔplkA::pyroA; spa10(p)::spa10::GFP::AfpyrG* (SRM212 transformed with pXL79, homologous integration)	This work
CDS449	*wA3, AnNup49-GFP::pyrGAf; histone H1-mRFP1::pyrG; pabaA1; fwA1*	Stephen Osmani (Ohio State Univ.)
SSH167	*CDS449 crossed to 65; wA3; alcA(p)::GFP-tubA; AnNup49-GFP; histone H1-mRFP1; pabA1*	This work
SSH168	*SSH167 crossed to SXL122; alcA(p)::GFP-tubA; AnNup49-GFP; histone H1-mRFP1; □plkA*	This work
SSH169	*CDS449 crossed to 65; wA3; alcA(p)::GFP-tubA; histone H1-mRFP1; pyroA4*	This work
SSH171	*pyrG89; plkA(p)::GFP-plkA::pyr-4 argB2; pyroA4, ΔnkuA::argB; veA1* (TN02A3 transformed with pSH108)	
SSH172	*Heterokaryon SXL80 x SXL137; pyrG89; argB2; pyroA4, ΔnkuA::argB; plkA(p)::plkA::GFP::AfpyrG; alcA(p)::mCherry::pcpA::pyroA*	This work

Table S3. List of yeast strains used in this study

Strain	Genotype	Source
AH109	MAT*a*; *trp1-901*; *leu2-3*, *112*; *ura3-52*; *his3-200*; *gal4*Δ; *gal80*Δ; *LYS2*::*GAL1*$_{UAS}$-*GAL1*$_{TATA}$-*HIS3*; *GAL2*$_{UAS}$-*GAL2*$_{TATA}$-*ADE2*; *URA3*::*MEL1*$_{UAS}$-*MEL1*$_{TATA}$-*lacZ*	(James et al., 1996)
Y187	*MATα*; *ura3-52*; *his3-200*; *ade2-101*; *trp1-901*; *leu2-3*; *112*; *gal4*Δ; *met-*; *gal80*Δ; *URA3*::*GAL1*$_{UAS}$-*GAL1*$_{TATA}$-*lacZ*	(Harper et al., 1993)
AH109_ AD-ApsB	AH109 transformed with pRS88; Gal4 AD-ApsB	This work
Y187_ BD-PlkA	Y187 transformed with pXL111; Gal4 BD-PlkA	This work
AH109_ AD-PlkA	AH109 transformed with pXL112; Gal4 AD-PlkA	This work
Y187_ BD-ApsB	Y187 transformed with pRS89; Gal4 BD-ApsB	This work
Y2H_AD-ApsB/BD-PlkA	AH109 mated with Y187; Gal4 AD-ApsB; Gal4 BD-PlkA	This work
Y2H_AD-PlkA/BD-ApsB	AH109 mated with Y187; Gal4 AD-PlkA; Gal4 BD-ApsB	This work
Y2H_AD-PlkA/BD-PlkA	AH109 mated with Y187; Gal4 AD-PlkA; Gal4 BD-PlkA	This work
Y2H_AD-ApsB/BD-ApsB	AH109 mated with Y187; Gal4 AD-ApsB; Gal4 BD-ApsB	This work
AH109_ AD-GcpC	AH109 transformed with pJA5; Gal4 AD-GcpC	This work

Y187_ BD-GcpC	Y187 transformed with pJA6; Gal4 BD-GcpC	This work
AH109_ AD-PcpA^{Smc}	AH109 transformed with pXL125; Gal4 AD-PcpA^{Smc}	This work
Y187_ BD-PcpA^{Smc}	Y187 transformed with pXL126; Gal4 BD-PcpA^{Smc}	This work
Y2H_AD-GcpC/BD-PlkA	AH109 mated with Y187; Gal4 AD-GcpC; Gal4 BD-PlkA	This work
Y2H_AD-PlkA/BD-GcpC	AH109 mated with Y187; Gal4 AD-PlkA; Gal4 BD-GcpC	This work
Y2H_AD-PcpA^{Smc}/BD-PlkA	AH109 mated with Y187; Gal4 AD-PcpA^{Smc}; Gal4 BD-PlkA	This work
Y2H_AD-PlkA/BD-PcpA^{Smc}	AH109 mated with Y187; Gal4 AD-PlkA; Gal4 BD-PcpA^{Smc}	This work
Positive control	AH109 transformed with pGADT7-T and pGBKT7-53	This work
Negative control	AH109 transformed with pGADT7-T and pGBKT7-Lam	This work

Table S4. List of plasmids used in this study

Plasmid	Genotype	Source
pJET1.2/blunt	Blunt end cloning vector	Fermentas
pMCB17apx	*alcA(p)*::*GFP*, for N-terminal fusion of GFP to proteins of interest; contains *N. crassa pyr4*	(Efimov et al., 2006)
pFNO3	*$(GA)_5$::GFP::AfpyrG*, Kan^r, Amp^r	Fungal Genetic Stock Center, MO
pGADT7-Rec	Gal4 DNA-activation domain (AD); Amp^r	Clontech
pGBKT7	Gal4 DNA-binding domain (BD); Kan^r	Clontech
pSH44	*alcA(p)::mCherry::alpha tubulin*, *pyroA*, Amp^r (pMCB17apx with 3.1 kb *alpha tubulin*)	(Manck et al., 2015)
pSK82	*alcA(p)::GFP::kipA*, *pyr4*, Amp^r (pMCB17apx with 1 kb *kipA*)	(Konzack et al., 2005)
pYZ59	*alcA(p)::YFP^N::apsB*, *pyroA*, Amp^r (pMCB17apx with full length *apsB*)	(Zhang et al., 2017)
pXL23	pJET1.2/blunt with *mztA(C-terminal)::GFP::AfpyrG::mztA(RB)*	(Gao et al., 2019)
pXL32	*alcA(p)::GFP::tubA*, *pyr4*, Amp^r (pMCB17apx with 3.1kb *tubA*)	(Gao et al., 2019)
pXL58	*alcA(p)::YFP^N::pcpA*, *pyroA*, Amp^r (pMCB17apx with 1kb *pcpA*)	(Gao et al., 2019)
pRS89	pGBKT-7 with apsB cDNA, Kan^r	R. Suelmann, Marburg

pRS88	pGADT-7 with apsB cDNA, Amp^r	R. Suelmann, Marburg
pXW8	*alcA(p)::YFP^C::plkA*, *pyr4*, Amp^r (pMCB17apx with 1 kb *plkA, YFP^C* instead of *GFP*)	This work
pXL79	pJET1.2/blunt with *plkA(LB)::pyroA::plkA(RB)* deletion cassette	This work
pXL81	pJET1.2/blunt with *plkA(p)::plkA::AfpyrG* complementation cassette	This work
pXL82	pJET1.2/blunt with *plkA(C-ter)::GFP::AfpyrG::plkA(RB)* cassette	This work
pXL83	*alcA(p)::mCherry::plkA*, *pyroA*, Amp^r (pMCB17apx with 1kb *plkA*)	This work
pXL84	*alcA(p)::GFP::plkA*, *pyr4*, Amp^r (pMCB17apx with 1kb *plkA*)	This work
pXL102	pJET1.2/blunt with plkA exon cassette	This work
pXL106	*alcA(p)::GFP::apsB*, *pyr4*, Amp^r (pMCB17apx with full length of ApsB)	This work
pXL107	*alcA(p)::GFP::apsB$^{1414S\ to\ A}$*, *pyr4*, Amp^r (pMCB17apx with mutated full length of ApsB)	This work
pXL108	*alcA(p)::GFP::apsB$^{1414S\ to\ D}$*, *pyr4*, Amp^r (pMCB17apx with mutated full length of ApsB)	This work
pXL109	*alcA(p)::GFP::apsB$^{321S\ to\ A}$*, *pyr4*, Amp^r (pMCB17apx with mutated full length of ApsB)	This work
pXL110	*alcA(p)::GFP::apsB$^{321S\ to\ D}$*, *pyr4*, Amp^r (pMCB17apx with mutated full length of ApsB)	This work
pXL111	pGBKT-7 with full length of plkA cDNA, Kan^r	This work

pXL112	pGADT-7 with full length of plkA cDNA, Amp^r	This work
pJA5	pGADT-7 with gcpC cDNA, Amp^r	This work
pJA6	pGBKT-7 with gcpC cDNA, Kan^r	This work
pXL114	*alcA(p)::mCherry::plkA*$^{95\ K\ to\ R}$, *pyroA*, Amp^r (pMCB17apx with 1kb mutated *plkA*)	This work
pXL117	*alcA(p)::GFP::apsB*$^{327S\ to\ A}$, *pyr4*, Amp^r (pMCB17apx with mutated full length of ApsB)	This work
pXL118	*alcA(p)::GFP::apsB*$^{327S\ to\ D}$, *pyr4*, Amp^r (pMCB17apx with mutated full length of ApsB)	This work
pXL123	*alcA(p)::GFP::apsB*$^{321S\ to\ A;\ 327S\ to\ A\ ;\ 1414S\ to\ A}$, *pyr4*, Amp^r (pMCB17apx with mutated full length of ApsB)	This work
pXL124	*alcA(p)::GFP::apsB*$^{321S\ to\ D;\ 327S\ to\ D\ ;\ 1414S\ to\ D}$, *pyr4*, Amp^r (pMCB17apx with mutated full length of ApsB)	This work
pXL125	pGADT-7 with Smc domain of PcpA, Amp^r	This work
pXL126	pGBKT-7 with Smc domain of PcpA, Kan^r	This work
pSH108	*plkA(p)::GFP-plkA* full length in pMBC17apx	This work

Table S5. Oligonucleotides used in this work.

Name	Sequence 5'-3'
***plkA* deletion**	
plkA-LB_fwd	CGTCATCCCTTCGGTTATTCT
plkA-LB-pyroA linker_rev	ATGGTCTCGAACTGACCTTACGGTTCTCGAACAAATGCGG
pyroA_fwd	GTAAGGTCAGTTCGAGACCA
pyroA_rev	TGCATCAAAGAACGCTATATCAAC
plkA-RB-pyroA linker_fwd	GTTGATATAGCGTTCTTTGATGCAGACTGATGACCTTGGGTTGT
plkA-RB_rev	ACAGGCAATGCAAAGAACTG
plkA-LB-N-fwd	GATGAAAGTTGCGCCTGATT
plkA-RB-N_rev	GAGAGGAAAACAGATCGGCT
PlkA C-terminal localization	
plkA-C-termi_fwd	TAACTTGGTTCCTGGTTCGG
plkA-C-termi_GA linker_rev	CAGCGCCTGCACCAGCTCCTAAGCCCGCTAATCGCAG
GA linker_fwd	GGAGCTGGTGCAGGCGCTG
pyrG overhang_rev	CTGTCTGAGAGGAGGCACTGAT
plkA-RB-pyrG linker_fwd	ATCAGTGCCTCCTCTCAGACAGGACTGATGACCTTGGGTTGT
plkA-RB_rev	ACAGGCAATGCAAAGAACTG
plkA-C-termi-N_fwd	CATGCGTATGTCATCAAGTGG
plkA-RB-N_rev	GAGAGGAAAACAGATCGGCT

PlkA N-terminal localization	
plkA_AscI_fwd	A*GGCGCGCC*AATGGAGAGACACCTCCAAC
plkA_PacI_rev	CC*TTAATTAA*GTCAAAATCTAGGCCATGGC
***plkA* re-complementation**	
plkA-promo_builder_fwd	CTCGAGTTTTTCAGCAAGATAATCATCCTTATTCGTTGACCAAG
plkA-termi_pyrG linker_rev	GAAGAGCATTGTTTGAGGCGTGGGATCGAGAATTGGGG
pyrG_fwd	CGCCTCAAACAATGCTCTTC
pyrG builder_rev	AGGAGATCTTCTAGAAAGATCTGTCTGAGAGGAGGCACTGAT
PlkA cDNA for Y2H	
plkA-CDS1_builder_fwd	CTCGAGTTTTTCAGCAAGATATGGAGAGACACCTCCAAC
plkA-CDS1_CDS2 linker_rev	TCTGCAGCTCTGTTCGAAACTTCTCTTGCATCTTTTTCTGGC
plkA-CDS2_fwd	TTTCGAACAGAGCTGCAGA
plkA-CDS2_rev	CAGATCACTCCCAGGGAC
plkA-CDS3_CDS2 linker_fwd	GTCCCTGGGAGTGATCTGTTTTGCAATGCTTACGGGATAT
plkA-CDS3_builder_rev	AGGAGATCTTCTAGAAAGATTAAGCCCGCTAATCGCAG
plkA *Nde*I AD/BD_fwd	GGAATTCCATATGATGGAGAGACACCTCCAAC
plkA *Xma*I AD/BD_rev	TCCCCCCGGGTAAGCCCGCTAAACGCAG
***plkA* catalytic mutation**	
plkA_95K/R_fwd	CTTTGCAATGAGAGTCGTAAAGTCTGACATG
plkA_95K/R_rev	ACACGACCGTTGCGCAAC

plkA_95 seq_fwd	ATGGAGAGACACCTCCAAC
PcpA^{Smc} cDNA for Y2H	
pcpA^{Smc}_*Nde*I AD/BD_fwd	GGAATTCCATATGGACCAGCGCGTGAAAGAA
pcpA^{Smc}_ *Xma*I AD/BD_rev	TCCCCCCGGGTTTCTTGATCGTGGCATCGT
GcpC cDNA for Y2H	
gcpC-CDS1_builder_fwd	CTCGAGTTTTTCAGCAAGATATGTCAAGTCGGCACCAT
gcpC-CDS1_CDS2 linker_rev	TAATTGACCTCCTTTCTTGCTCTGAGCCTCCTCAACAAT T
gcpC-CDS2_fwd	GCAAGAAAGGAGGTCAATTAGTG
gcpC-CDS2_buildDCer_rev	AGGAGATCTTCTAGAAAGATTTGCTCAGTCGAATCCTTC TT
gcpC_*Xma*I_BD_fwd	TCCCCCCGGGATGTCAAGTCGGCACCAT
gcpC_*Not*I_BD_rev	ATAGTTTAGCGGCCGCTTGCTCAGTCGAATCCTTCTT
gcpC _SMARTII_AD _fwd	ACGCAGAGTGGCCATTATGGATGTCAAGTCGGCACCAT
gcpC _CDSIII_AD _rev	AGGCCGAGGCGGCCGACATGTTGCTCAGTCGAATCCTT CT
ApsB phosphor-mutant	
apsB-321S/A_fwd	TGGCAATGTCGCCGATGCGGATG
apsB-321S/A_rev	TCACTAAATAGTTTGGTGTG
apsB-327S/A_fwd	GGATGCCGCAGCTCGCAGAGGTA
apsB-327S/A_rev	GCATCGCTGACATTGCCATCACTAAATAG
apsB-1414S/A_fwd	CGTGGCAGGCGCGCCGCAGTCAT
apsB-1414S/A_rev	CCAGCTGTCGTGCTGCGGC

apsB-321S/A,327S/A_fwd	TGCCGCAGCTCGCAGAGGTAGCCGAAGG
apsB-321S/A,327S/A_rev	TCCGCATCGGCGACATTGCCATCACTAAATAGTTTGG
apsB-321S/D_fwd	TGGCAATGTCGACGATGCGGATG
apsB-321S/D_rev	TCACTAAATAGTTTGGTGTG
apsB-327S/D_fwd	GGATGCCGCAGATCGCAGAGGTAG
apsB-327S/D_rev	GCATCGCTGACATTGCCA
apsB-1414S/D_fwd	CGTGGCAGGCGACCCGCAGTCATCCAC
apsB-1414S/D_rev	CCAGCTGTCGTGCTGCGG
apsB-321S/D,327S/D_fwd	TGCCGCAGATCGCAGAGGTAGCCGAAGG
apsB-321S/D,327S/D_rev	TCCGCATCGTCGACATTGCCATCACTAAATAGTTTGG
apsB-321,327 seq_fwd	CACGCCTTAGACTTCACAGA
apsB-1414 seq_fwd	ACCAGCCTTGAGCAACAG
confirmation of *plkA* deletion	
plkA-dele_check_fwd	CGTCATCCCTTCGGTTATTCT
plkA-ORF_rev	ATTTTCGCGCAGTTCCATC
plkA-RB_rev	ACAGGCAATGCAAAGAACTG
confirmation of N-terminal homologous integration	
alcA check_fwd	AGACGGAGCACTTTCTGG
apsB 1kb Int check_rev	CCAGATGCCATACTTCCCAA
plkA 1kb Int check_rev	ATTTTCGCGCAGTTCCATC
pcpA 1kb Int check_rev	CCTCCAGCTGTTCTTTTGC
confirmation of C-terminal	

homologous integration	
pyrG check_fwd	CGCCTCAAACAATGCTCTTC
plkA C-termi check_rev	ACAGGCAATGCAAAGAACTG
mztA C-termi check_rev	TCACGAATCACGGGAAGG
gcpC C-termi check_rev	ACCGTCATGGCAGAAACGAAG

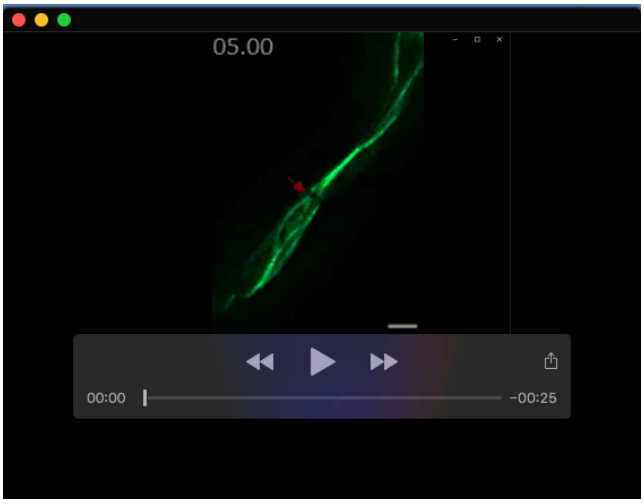

Movie 1. GFP-TubA interphase at septa in wild type. Strain SJW02 (*alcA(p)::GFP::tubA*) was cultured in 8 well u-slides at 28°C overnight. Arrows marked septum positions. Time-lapse interval was 5s in the 30-frames movie. The length of the movie was 6s and the speed 5fps. Scale bar, 2μm.

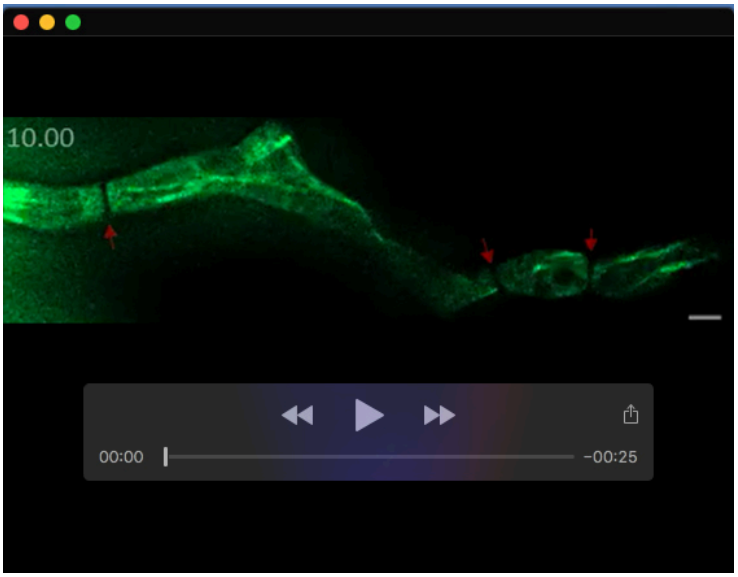

Movie 2. GFP-TubA interphase at septa in the Δ*plkA*-deletion mutant. SXL177 (Δ*plkA, alcA(p)::GFP::tubA*) was cultured in 8 well u-slides at 28°C overnight. Arrows marked septum positions. Time-lapse interval was 10s in the 12-frames movie. The length of the movie was 4s and the speed 3fps. Scale bar, 2μm.

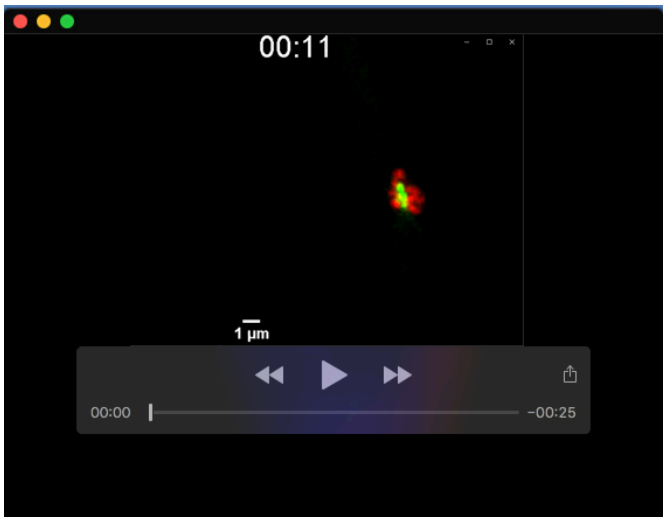

Movie 3. Visualization of mitosis in WT. Strain: *(alcA(p)::mRFP::H1,alcA(p)::GFP::tubA*). Excitation laser wavelengths were 488 for GFP and 561 nm for mRFP. Fluorescence signals were detected using the Airy scan detector with SR (super resolution) mode (Weisshart, 2014 *ZEISS Technology Note*). Images were collected using the ZEN blue software (ZEISS).

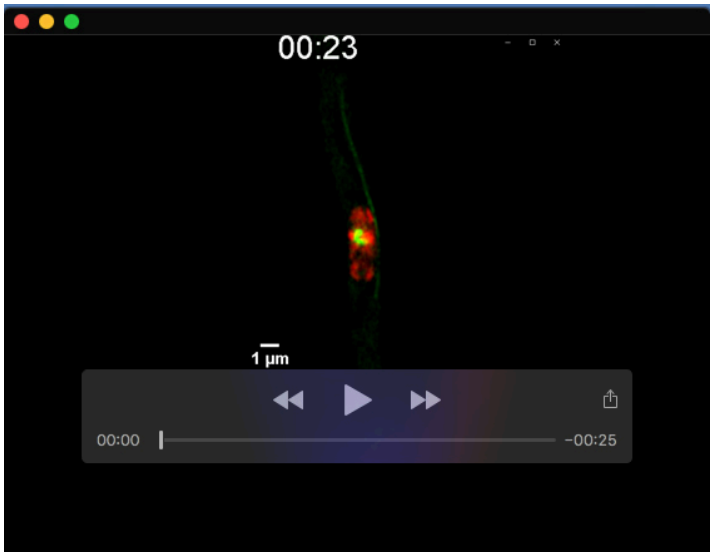

Movie 4. Visualization of mitosis in the Δ*plkA*-deletion strain. Strain: (Δ*plkA, alcA(p)::mRFP::H1, alcA(p)::GFP::tubA*). Excitation laser wavelengths were 488 for GFP and 561 nm for mRFP. Fluorescence signals were detected using the Airy scan detector with SR (super resolution) mode (Weisshart, 2014 *ZEISS Technology Note*). Images were collected using the ZEN blue software (ZEISS).

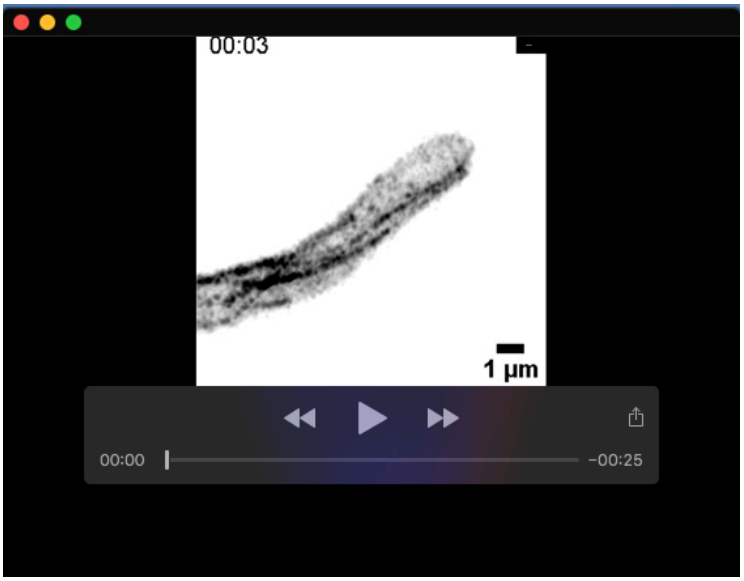

Movie 5. MT dynamics in WT. Imaging for 1:34 min (WT) and 1 min (Δ*plkA*-deletion mutant) using the Airy scan detector in Multiplex 4Y mode.

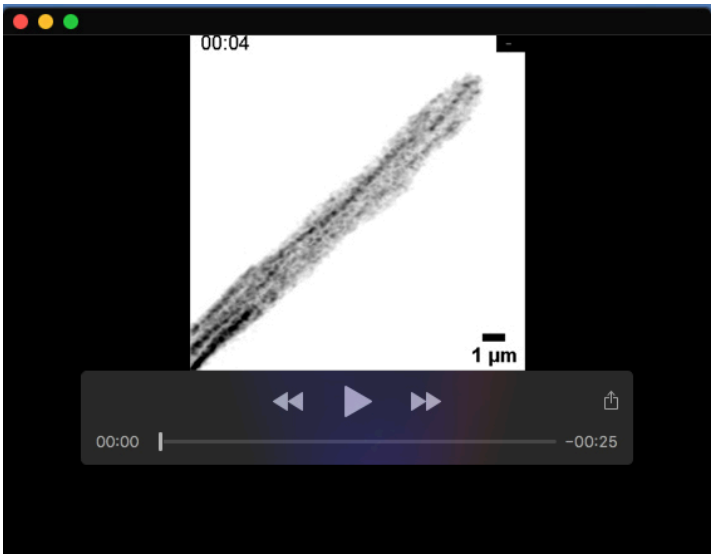

Movie 6. MT dynamics in the Δ*plkA*-deletion strain. Imaging for 1:34 min (WT) and 1 min (Δ*plkA*-deletion mutant) using the Airy scan detector in Multiplex 4Y mode.